





## Research Article

# Nonlinear Dynamics in the Coupled Fractional-Order Memristor Chaotic System and Its Application in Image Encryption

Sarah Alharbi <sup>1</sup>, Amr Elsonbaty <sup>1,2</sup>, A. A. Elsadany <sup>1,3</sup> and Fatma Kamal <sup>2</sup>

<sup>1</sup>Department of Mathematics, College of Science and Humanities in Al-Kharj, Prince Sattam Bin Abdulaziz University, Al-Kharj 11942, Saudi Arabia

<sup>2</sup>Mathematics and Engineering Physics Department, Faculty of Engineering, Mansoura University, Mansoura 35516, Egypt

<sup>3</sup>Department of Basic Science, Faculty of Computers and Informatics, Suez Canal University, Ismailia, Egypt

Correspondence should be addressed to Amr Elsonbaty; [sonbaty2010@gmail.com](mailto:sonbaty2010@gmail.com)

Received 31 August 2022; Revised 21 October 2022; Accepted 13 February 2023; Published 8 April 2023

Academic Editor: Akif Akgul

Copyright © 2023 Sarah Alharbi et al. This is an open access article distributed under the Creative Commons Attribution License, which permits unrestricted use, distribution, and reproduction in any medium, provided the original work is properly cited.

This work presents two forms of coupled fractional-order memristor chaotic systems. The existence and uniqueness of solutions are studied. Moreover, the range of parameters and time span at which the proposed two models exhibit continuous dependence on initial conditions are examined. The unique equilibrium point for each system is found, and the corresponding stability analysis is carried out. The regions of stability in the space of parameters are obtained, whereas numerical simulations are employed to confirm theoretical results. The bifurcation diagrams, in addition to Lyapunov exponents, are utilized to examine the effects of key parameters in two models. A chaos-based encryption scheme is presented as an application to utilize complicated chaotic behaviors in coupled circuits.

## 1. Introduction

Several phenomena that are subject to spatio-temporal development have been encountered in various fields of application, such as physics, engineering, biology, economy, and chemistry [1, 2]. To better study and interpret emerging nonlinear phenomena, the theories of dynamical systems and chaos are helpful tools that achieve these goals. The applications of dynamical systems and chaos have been involved in many disciplines such as electronic circuits [3, 4], chaos and synchronization [5–8], mathematical biology [1], image encryption [9], secure communications [10], cryptography [11], and neuroscience research [12].

Nonlinear electronic circuits can be considered a very useful practical tool for studying nonlinear phenomena and chaos. This line of research has attracted considerable interest, especially due to the works of L.O. Chua from the mid-1960s. Chua proposed a resistor with two terminals having a piecewise-continuous voltage-current characteristic referred to as Chua's diode, and Chua's circuit is the name of the resulting circuit [13]. Since then, several

developments have been introduced in the field of nonlinear circuits. For instance, Shinriki et al. inserted a nonlinear circuit called the modified Van der Pol oscillator (MVPO) [14]. King and Gaito derived a nonlinear circuit based on the MVPO circuit and called this circuit an autonomous Van der Pol–Duffing (ADVP) oscillator [15]. A modification to the ADVP circuit was conducted through adding a resistor in parallel with the inductor in the baseline ADVP circuit [16]. In the modified ADVP, the dynamics of the original ADVP oscillator are confined in a small range of the circuit's parameter.

Chua theoretically forecasted the memristor as a fundamental fourth circuit component in 1971. The memristor is a nonlinear two-terminal component, in which the induced magnetic flux is the function of an electric charge that passes through the device [17, 18]. The memristor has taken its place along with other conventional circuit components, which include the resistor, capacitor, and inductor, when Williams et al. [18] fabricated the first solid-state implementation of memristor circuit components. There are many important applications of memristors such as learning

networks, ultradense nonvolatile memories, high-frequency oscillators, and secure communications applications employing nanoscale memristor-based circuits [18–21].

The multistability analysis of a novel memristor-based chaotic circuit has been introduced in [22] along with circuit implementations and application in image encryption. Examples of chaotic dynamics in biological systems and chaos-based image encryption schemes can be found in [23–25] and references therein.

Recently, the applications of fractional calculus in mathematical modeling of dynamical systems have attracted increasing attention. Several theoretical and experimental studies have indicated that fractional-order derivatives are more adequate and can provide accurate mathematical models of intricate systems with memory, in contrast to classical integer-order models [26]. Fractional-order differential equations have been verified as the more appropriate modeling tool for several real problems in many fields of science, engineering [26], biological systems [27, 28], economic systems [29, 30], circuit theory [31, 32], and many more. The chaotic behavior has also been found in many fractional-order systems [33], such as fractional Lu systems [34] and fractional Lorenz systems [35]. From an application point of view, chaotic systems are widely used to design algorithms dedicated to image encryption [36–39]. Indeed, fractional-order chaotic systems have good advantages in terms of pseudorandomness and ergodicity and are extremely sensitive to initial conditions which are very appropriate for image encryption [40]. Synchronization of fractional chaotic systems and its applications in encryption of images have been presented in [41]. In addition, the improper fractional-order laser chaotic system and its application for image encryption are considered in [42].

Fractional-order differential equations are known to better model natural, engineering, and physical systems having memory characteristics. On the other hand, the fourth basic circuit element, i.e., the memristor, relates the values of the flux across its terminals with the past values (history) of the current passed through it. In other words, the memristor can memorize the history of its state. So it is more adequate to employ fractional-order differential equations with memristor-based circuits. The other point which motivates this work is to examine the more general case where coupled fractional-order chaotic memristor-based circuits are established. Indeed, there are some interesting questions which arise and need to be investigated, for example, what are the influences of the fractional order and type of coupling on the dynamical characteristics and equilibrium points and their stability in the coupled system. Finally, it is also essential to explore which potential applications can be established based on the analytical/theoretical results obtained in the study. The paper is an attempt to explore the answers to these questions. Due to the distinct characteristics of memristors, they are crucial elements in chaotic circuits with very small sizes and low-power consumption. Therefore, the present work establishes theoretical/numerical frameworks for practical studies which implement memristors in efficient image encryption

hardware. The proposed image encryption method, on the other hand, creates chaotic sequences which depend on tiny changes in both secret keys and input plain images. This implies that the proposed scheme can resist known-plaintext attacks, known-ciphertext attacks, and differential attacks, while it can be realizable in small, very fast, and low-power-consumed appliances.

With the rapid development of the Internet and wireless communication systems, images and real-time videos are considered among the most important carriers of information. So ensuring the security of transmission, storage and access to digital images has become a very active topic for researchers. From a mathematical point of view, the fascinating features of chaotic dynamics attracted the attention of mathematicians, engineers, and computer scientists. More specifically, chaos has the characteristics of random-like behavior, unpredictability, ergodicity, sensitive dependence on parameters and initial values, and the ability to produce very complicated behaviors from relatively simple-structure systems, which render chaotic systems an ideal choice in the field of image encryption. Chaotic systems also have the advantages of being easily realizable on field-programmable gate arrays (FPGAs), digital signal processors (DSPs), or microcontrollers. In addition, they can be included in ultrafast secure communication systems which utilize chaotic semiconductor lasers or ring fiber lasers. Some of the recent developments in the field of chaos-based cryptography can be seen in [43–49].

In this work, two forms of coupled fractional-order memristor chaotic systems along with the study of the existence and uniqueness of the proposed model's solution and conditions of continuous dependence on initial conditions are presented in Section 2. The stability analysis of the unique equilibrium point for each system is presented in Section 3. The regions of stability in the space of parameters are obtained, and numerical simulations are employed to verify the theoretical results. In Section 4, the bifurcation diagrams and Lyapunov exponents are employed to inspect the effects of key parameters in the two systems. Finally, a chaos-based encryption scheme is presented in Section 5 as an application to utilize complicated chaotic behaviors in the coupled circuit.

## 2. The Proposed Coupled Fractional-Order System

In this section, two forms of coupling are introduced for the proposed coupled fractional-order memristor-based chaotic system, namely, partial coupling and complete coupling cases. First, some key definitions and properties of fractional calculus have been reviewed.

*Definition 1.* The fractional-order integral of the order  $\gamma \in R^+$  for a function  $h(t)$ ,  $t \geq \sigma$  is defined by ([50–52])

$$I_{\sigma}^{\gamma} h(t) = \int_{\sigma}^t \frac{(t-s)^{\gamma-1}}{\Gamma(\gamma)} f(s) ds. \quad (1)$$

*Definition 2.* The Caputo fractional-order derivative with the order  $\zeta \in (n - 1, n)$  of  $k(t), t \geq \sigma$  is defined by

$$D_{\sigma}^{\zeta} k(t) = I_{\sigma}^{n-\zeta} D^n k(t), D = \frac{d}{dt}. \quad (2)$$

For main properties of fundamental fractional-order derivatives and integrals, the readers are referred to see [50–60].

Memristors can be classified as flux-controlled or charge-controlled memristors. In flux-controlled memristors, the charge  $q$  is related to the flux  $\phi$  of the memristor by the relation

$$q(\phi) = G(\phi), \quad (3)$$

where  $G$  is a flux-dependent function. By differentiating the above equation w.r.t. time, it yields

$$i(t) = W(\phi)v(t), \quad (4)$$

where  $i(t)$  denotes the current that passes through the memristor,  $v(t)$  is the voltage across its terminals, and  $W(\phi)$  refers to the incremental memductance function which describes the change rate of the charge with flux. In particular,

$$W(\phi) = \frac{dq(\phi)}{d\phi}. \quad (5)$$

Similarly, the second type of memristors is the charge-controlled memristor which can be described by the following equations:

$$\begin{aligned} \phi(q) &= K(q), \\ v(t) &= \frac{d\phi(q)}{dq} i(t). \end{aligned} \quad (6)$$

In this work, the flux-controlled memristor is used.

For the proposed partial coupling case, the system is described as

$$\begin{aligned} D^{\xi} x_1(t) &= -\gamma x_1 + \sigma y_1 - x_1 w_1^2 + \epsilon(w_2 - \delta x_1), \\ D^{\xi} y_1(t) &= \alpha x_1 - y_1 - z_1 + \epsilon(z_2 - \delta y_1), \\ D^{\xi} z_1(t) &= \beta y_1, \\ D^{\xi} w_1(t) &= x_1, \\ D^{\xi} x_2(t) &= -\gamma x_2 + \sigma y_2 - x_2 w_2^2 + \epsilon(\delta x_2 - w_1), \\ D^{\xi} y_2(t) &= \alpha x_2 - y_2 - z_2, \\ D^{\xi} z_2(t) &= \beta y_2, \\ D^{\xi} w_2(t) &= x_2. \end{aligned} \quad (7)$$

For the complete coupling case, the system is proposed in the form

$$\begin{aligned} D^{\xi} x_1(t) &= -\gamma x_1 + \sigma y_1 - x_1 w_1^2 + \epsilon(w_2 - \delta x_1), \\ D^{\xi} y_1(t) &= \alpha x_1 - y_1 - z_1 + \epsilon(z_2 - \delta y_1), \\ D^{\xi} z_1(t) &= \beta y_1 + \epsilon(y_2 - \delta z_1), \\ D^{\xi} w_1(t) &= x_1 + z_2, \\ D^{\xi} x_2(t) &= -\gamma x_2 + \sigma y_2 - x_2 w_2^2 + \epsilon(\delta x_2 - w_1), \\ D^{\xi} y_2(t) &= \alpha x_2 - y_2 - z_2 + \epsilon(z_1 - \delta y_2), \\ D^{\xi} z_2(t) &= \beta y_2 + \epsilon(y_1 - \delta z_2), \\ D^{\xi} w_2(t) &= x_2 + z_1. \end{aligned} \quad (8)$$

Systems (7) and (8) are coupled systems of two fractional-order chaotic memristor circuits. The circuit is illustrated in Figure 1 and consists of two resistors, two capacitors, one inductor, and the memristor element. The generalization to the fractional-order case is introduced, and the different cases of couplings are examined from theoretical/numerical viewpoints along with image encryption applications.

*2.1. Existence and Uniqueness.* The proposed system (7) can be expressed in the following form:

$$\begin{aligned} D^{\xi} X(t) &= \Psi(X(t)), \\ t &\in (0, T], \end{aligned} \quad (9)$$

for  $X(t) = [x_1 \ y_1 \ z_1 \ w_1 \ x_2 \ y_2 \ z_2 \ w_2]^T$  with initial conditions  $X(0) = X_0$ .

The solution of this initial value problem is therefore obtained by

$$X(t) = X_0 + \int_0^t \frac{(t-\theta)^{\xi-1}}{\Gamma(\xi)} \Psi(X(\theta)) d\theta. \quad (10)$$

The existence of this solution is examined in the region  $\Pi \times J$  where

$$\begin{aligned} \Pi &= \{ \{\omega_i\} : \max [|\omega_i|] < K \}, \\ J &= (0, T], \end{aligned} \quad (11)$$

$\omega = x, y, z, w$  and  $i = 1, 2, 3, 4$ . The equivalence between the above integral (10) and original system (7) is utilized as follows.

The right hand side of (10) is referred to as  $\Omega(X)$ , and hence, we obtain

$$\begin{aligned} \Omega(X_1) - \Omega(X_2) &= \int_0^t \frac{(t-\theta)^{\xi-1}}{\Gamma(\xi)} (\Psi(X_1(\theta)) - \Psi(X_2(\theta))) d\theta, \\ |\Omega(X_1) - \Omega(X_2)| &\leq \int_0^t \left| \frac{(t-\theta)^{\xi-1}}{\Gamma(\xi)} (\Psi(X_1(\theta)) - \Psi(X_2(\theta))) \right| d\theta. \end{aligned} \quad (12)$$

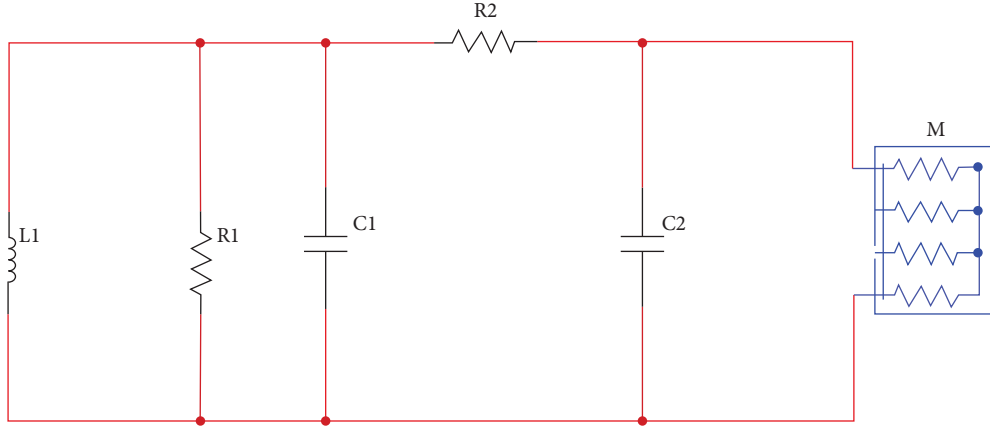


FIGURE 1: Schematic diagram of the chaos-based memristor circuit.

The following inequality can be obtained after some calculations:

$$\|\Omega(X_1) - \Omega(X_2)\| \leq \Lambda \|X_1 - X_2\|, \quad (13)$$

$$\Lambda = \frac{T^\xi}{\Gamma(\xi + 1)} \max \{K^2 + |\epsilon\delta| + |\alpha| + |\gamma| + 1, |\beta| + |\sigma| + 1, 2K^2 + |\epsilon|\}.$$

Here, the supremum norm is employed for the class  $C^1$  of differentiable continuous functions on  $J$ .

Now, we get the following theorem which states the sufficient condition for existence and uniqueness of system (7).

**Theorem 1.** Assume that  $\Lambda = T^\xi/\Gamma(\xi + 1) \max \{K^2 + |\epsilon\delta| + |\alpha| + |\gamma| + 1, |\beta| + |\sigma| + 1, 2K^2 + \epsilon\} < 1$ , then the solution of system (3) exists, and it is unique on  $\Pi \times J$ .

*Proof.* For  $\Lambda < 1$ , the mapping  $X = \Psi(X)$  is a contraction mapping, and the theorem follows immediately from the Banach fixed-point theorem.

On the other side, the second proposed system (8) is expressed as

$$D^\xi X(t) = Y(X(t)), \quad (14)$$

$$t \in (0, T],$$

for  $X(t) = [x_1 \ y_1 \ z_1 \ w_1 \ x_2 \ y_2 \ z_2 \ w_2]^T$  and the initial conditions  $X(0) = X_0$ .

The solution of the initial value problem is written as

$$X(t) = X_0 + \int_0^t \frac{(t-\theta)^{\xi-1}}{\Gamma(\xi)} Y(X(\theta)) d\theta. \quad (15)$$

The existence of the solution is examined in the region  $\Pi \times J$  where

$$\Pi = \{\omega_i : \max [|\omega_i|] < K\}, \quad (16)$$

$$J = (0, T],$$

$\omega = x, y, z, w$  and  $i = 1, 2, 3, 4$ . The equivalence between the above integral (15) and original system (8) is employed as follows.

The right hand side of (15) is referred to as  $\Phi(X)$ , and hence, we obtain

$$\Phi(X_1) - \Phi(X_2) = \int_0^t \frac{(t-\theta)^{\xi-1}}{\Gamma(\xi)} (Y(X_1(\theta)) - Y(X_2(\theta))) d\theta,$$

$$|\Phi(X_1) - \Phi(X_2)| \leq \int_0^t \left| \frac{(t-\theta)^{\xi-1}}{\Gamma(\xi)} ((X_1(\theta)) - Y(X_2(\theta))) \right| d\theta. \quad (17)$$

The following inequality can be obtained after some calculations:

$$\|\Phi(X_1) - \Phi(X_2)\| \leq \Delta \|X_1 - X_2\|, \quad (18)$$

$$\Delta = \frac{T^\xi}{\Gamma(\xi + 1)} \max \{K^2 + |\epsilon\delta| + |\alpha| + |\gamma| + 1, |\epsilon\delta| + |\epsilon| + |\beta| + |\sigma| + 1, 2K^2 + |\epsilon|\}.$$



Now, we get the following theorem which states the sufficient condition for existence and uniqueness of (8).  $\square$

**Theorem 2.** Assume that  $\Delta = T^\xi/\Gamma(\xi + 1) \max\{K^2 + |\epsilon\delta| + |\alpha| + |\gamma| + 1, |\epsilon\delta| + |\epsilon| + |\beta| + |\sigma| + 1, 2K^2 + |\epsilon|\} < 1$ , then the solution of system (8) exists, and it is unique on  $\Pi \times J$ .

*Proof.* The proof of Theorem 1 is extended to the case of the complete coupling case in Theorem 2.  $\square$

2.2. Continuous Dependence of Initial Conditions for the Solutions of Coupled Systems (7) and (8)

**Theorem 3.** Assume that the conditions of Theorem 1 (Theorem 2) are satisfied, then the solution of system (7) (system (8)) exhibits continuous dependence on initial conditions; i.e., for every  $\varrho > 0$ , there exists  $\kappa > 0$  such that for two initial conditions satisfying  $|X_{01} - X_{02}| < \kappa$ . The solution trajectories achieve  $|X_{01} - X_{02}| < \kappa$ .

*Proof.* Consider any two solutions of system (7) (system (8)) which evolve from two close initial conditions  $X_{01}$  and  $X_{02}$  in the way that

$$0 < |X_{01} - X_{02}| < \kappa. \tag{19}$$

Assume that the conditions of Theorem 1 (Theorem 2) are satisfied, thus

$$X_1(t) = X_{01} + \int_0^t \frac{(t-\theta)^{\xi-1}}{\Gamma(\xi)} \Psi(X_1(\theta)) d\theta, \tag{20}$$

$$X_2(t) = X_{02} + \int_0^t \frac{(t-\theta)^{\xi-1}}{\Gamma(\xi)} \Psi(X_2(\theta)) d\theta.$$

In view of these two equations, it is obvious that

$$\begin{aligned} \|X_1 - X_2\| &\leq \|X_{01} - X_{02}\| + \Lambda \|X_1 - X_2\|, \\ (1 - \Lambda) \|X_1 - X_2\| &\leq \|X_{01} - X_{02}\|, \end{aligned} \tag{21}$$

where  $0 < \Lambda < 1$  as stated above.

Let  $\varrho = \kappa/1 - \Lambda$ , then it holds that

$$0 < \|X_1 - X_2\| < \varrho, \tag{22}$$

whenever

$$0 < |X_{01} - X_{02}| < \kappa. \tag{23}$$

Note that, for system (8),  $\varrho$  is defined by  $\varrho = \kappa/1 - \Delta$ , and the proof is completed.  $\square$

3. Stability of the Equilibrium Point

The unique equilibrium point of the proposed two systems (7) and (8) is  $X^* = (0, 0, 0, 0, 0, 0, 0, 0)$ . The interesting point here is that the original uncoupled 4D system has a line of equilibria, i.e., an infinite number of nonisolated equilibrium points. Partial and complete couplings are found to eliminate these lines of equilibria in the way that only the origin equilibrium point persists.

The Jacobian matrix of the fractional-order model (7) at  $X^*$  is evaluated as follows:

$$J_1 = \begin{pmatrix} -\gamma - \delta\epsilon & \sigma & 0 & 0 & 0 & 0 & 0 & \epsilon \\ \alpha & -1 & -1 & 0 & 0 & 0 & 0 & 0 \\ 0 & \beta & 0 & 0 & 0 & 0 & 0 & 0 \\ 1 & 0 & 0 & 0 & 0 & 0 & 0 & 0 \\ 0 & 0 & 0 & -\epsilon & \delta\epsilon - \gamma & \sigma & 0 & 0 \\ 0 & 0 & 0 & 0 & \alpha & -1 & -1 & 0 \\ 0 & 0 & 0 & 0 & 0 & \beta & 0 & 0 \\ 0 & 0 & 0 & 0 & 1 & 0 & 0 & 0 \end{pmatrix}, \tag{24}$$

whereas the Jacobian matrix of the fractional-order model (8) at  $X^*$  is evaluated as follows:

$$J_2 = \begin{pmatrix} -\gamma - \delta\epsilon & \sigma & 0 & 0 & 0 & 0 & 0 & \epsilon \\ \alpha & -\delta\epsilon - 1 & -1 & 0 & 0 & 0 & \epsilon & 0 \\ 0 & \beta & -\delta\epsilon & 0 & 0 & \epsilon & 0 & 0 \\ 1 & 0 & 0 & 0 & 0 & 1 & 0 & 0 \\ 0 & 0 & 0 & -\epsilon & \delta\epsilon - \gamma & \sigma & 0 & 0 \\ 0 & 0 & \epsilon & 0 & \alpha & -\delta\epsilon - 1 & -1 & 0 \\ 0 & \epsilon & 0 & 0 & 0 & \beta & -\delta\epsilon & 0 \\ 0 & 1 & 0 & 0 & 1 & 0 & 0 & 0 \end{pmatrix}. \tag{25}$$

For system (7), the characteristic equation of  $J_1$  is obtained as follows:

$$\lambda^8 + a_1\lambda^7 + a_2\lambda^6 + a_3\lambda^5 + a_4\lambda^4 + a_5\lambda^3 + a_6\lambda^2 + a_7\lambda + a_8 = 0, \tag{26}$$

where

$$\begin{aligned} a_1 &= 2\gamma + 2, a_2 = -2\alpha\sigma + 2\beta + \gamma^2 + 4\gamma - \delta^2\epsilon^2 + 1, \\ a_3 &= -2\alpha\gamma\sigma - 2\alpha\sigma + 4\beta\gamma + 2\beta + 2\gamma^2 + 2\gamma - 2\delta^2\epsilon^2, \\ a_4 &= \alpha^2\sigma^2 - 2\alpha\beta\sigma - 2\alpha\gamma\sigma + \beta^2 + 2\beta\gamma^2 + 4\beta\gamma - 2\beta\delta^2\epsilon^2 + \gamma^2 - \delta^2\epsilon^2 + \epsilon^2, \\ a_5 &= -2\alpha\beta\gamma\sigma + 2\beta^2\gamma + 2\beta\gamma^2 - 2\beta\delta^2\epsilon^2 + 2\epsilon^2, \\ a_6 &= \beta^2\gamma^2 - \beta^2\delta^2\epsilon^2 + 2\beta\epsilon^2 + \epsilon^2, a_7 = 2\beta\epsilon^2, a_8 = \beta^2\epsilon^2. \end{aligned} \tag{27}$$

On the other side, for system (8), the characteristic equation of  $J_2$  is obtained as follows: where

$$\lambda^8 + b_1\lambda^7 + b_2\lambda^6 + b_3\lambda^5 + b_4\lambda^4 + b_5\lambda^3 + b_6\lambda^2 + b_7\lambda + b_8 = 0, \quad (28)$$

$$\begin{aligned} b_1 &= 2\gamma + 4\delta\epsilon + 2, b_2 = -2\alpha\sigma + 2\beta + \gamma^2 + 8\gamma\delta\epsilon + 4\gamma + 5\delta^2\epsilon^2 + 6\delta\epsilon - 2\epsilon^2 + 1, \\ b_3 &= -2\alpha\gamma\sigma - 6\alpha\delta\sigma\epsilon - 2\alpha\sigma + 4\beta\gamma + 4\beta\delta\epsilon + 2\beta + 4\gamma^2\delta\epsilon + 2\gamma^2 + 12\gamma\delta^2\epsilon^2 + 12\gamma\delta\epsilon \\ &\quad - 4\gamma\epsilon^2 + 2\gamma + 4\delta^2\epsilon^2 - 4\delta\epsilon^3 + 2\delta\epsilon - 2\epsilon^2, \\ b_4 &= \alpha^2\sigma^2 - 2\alpha\beta\sigma - 6\alpha\gamma\delta\sigma\epsilon - 2\alpha\gamma\sigma - 6\alpha\delta^2\sigma\epsilon^2 + 2\alpha\delta\epsilon^2 - 4\alpha\delta\sigma\epsilon + 2\alpha\sigma\epsilon^2 - \beta^2\epsilon^2 + \beta^2 \\ &\quad + 2\beta\gamma^2 + 8\beta\gamma\delta\epsilon + 4\beta\gamma + 2\beta\delta\epsilon + 6\gamma^2\delta^2\epsilon^2 + 6\gamma^2\delta\epsilon - 2\gamma^2\epsilon^2 + \gamma^2 + 8\gamma\delta^3\epsilon^3 + 12\gamma\delta^2\epsilon^2 - 8\gamma\delta\epsilon^3 + 4\gamma\delta\epsilon \\ &\quad - 4\gamma\epsilon^2 - 5\delta^4\epsilon^4 - 4\delta^3\epsilon^3 - 2\delta\epsilon^3 + \epsilon^4, \\ b_5 &= 2\alpha^2\delta\sigma^2\epsilon - 2\alpha\beta\gamma\sigma - 2\alpha\beta\delta\sigma\epsilon - 6\alpha\gamma\delta^2\sigma\epsilon^2 - 4\alpha\gamma\delta\sigma\epsilon + 2\alpha\gamma\sigma\epsilon^2 - 2\alpha\delta^3\sigma\epsilon^3 + 6\alpha\delta^2\epsilon^3 \\ &\quad - 2\alpha\delta^2\sigma\epsilon^2 + 2\alpha\delta\sigma\epsilon^3 + 2\alpha\delta\epsilon^2 - 2\beta^2\gamma\epsilon^2 + 2\beta^2\gamma + 4\beta\gamma^2\delta\epsilon + 2\beta\gamma^2 + 4\beta\gamma\delta^2\epsilon^2 + 4\beta\gamma\delta\epsilon - 4\beta\delta^3\epsilon^3 \\ &\quad - 2\beta\delta^2\epsilon^2 + 4\gamma^2\delta^3\epsilon^3 + 6\gamma^2\delta^2\epsilon^2 - 4\gamma^2\delta\epsilon^3 + 2\gamma^2\delta\epsilon - 2\gamma^2\epsilon^2 + 2\gamma\delta^4\epsilon^4 + 4\gamma\delta^3\epsilon^3 - 4\gamma\delta^2\epsilon^4 \\ &\quad + 2\gamma\delta^2\epsilon^2 - 4\gamma\delta\epsilon^3 + 2\gamma\epsilon^4 - 2\gamma\epsilon^2 - 4\delta^5\epsilon^5 - 6\delta^4\epsilon^4 + 4\delta^3\epsilon^5 - 2\delta^3\epsilon^3 + 2\delta^2\epsilon^4 + 4\delta\epsilon^3 + 2\epsilon^2, \\ b_6 &= \alpha^2\delta^2\sigma^2\epsilon^2 - \alpha^2\epsilon^2 - 2\alpha\beta\gamma\delta\sigma\epsilon + 2\alpha\beta\delta\epsilon^2 - 2\alpha\gamma\delta^3\sigma\epsilon^3 - 2\alpha\gamma\delta^2\sigma\epsilon^2 + 2\alpha\gamma\delta\sigma\epsilon^3 + 6\alpha\delta^3\epsilon^4 \\ &\quad + 4\alpha\delta^2\epsilon^3 - 2\alpha\delta\epsilon^4 - \beta^2\gamma^2\epsilon^2 + \beta^2\gamma^2 + \beta^2\delta^2\epsilon^4 - \beta^2\delta^2\epsilon^2 + 2\beta\gamma^2\delta^2\epsilon^2 + 2\beta\gamma^2\delta\epsilon - 2\beta\delta^4\epsilon^4 - 2\beta\delta^3\epsilon^3 \\ &\quad + 2\beta\epsilon^2 + \gamma^2\delta^4\epsilon^4 + 2\gamma^2\delta^3\epsilon^3 - 2\gamma^2\delta^2\epsilon^4 + \gamma^2\delta^2\epsilon^2 - 2\gamma^2\delta\epsilon^3 + \gamma^2\epsilon^4 - \gamma^2\epsilon^2 - \delta^6\epsilon^6 - 2\delta^5\epsilon^5 + 2\delta^4\epsilon^6 \\ &\quad - \delta^4\epsilon^4 + 2\delta^3\epsilon^5 - \delta^2\epsilon^6 + 7\delta^2\epsilon^4 + 6\delta\epsilon^3 - 2\epsilon^4 + \epsilon^2, \\ b_7 &= -2\alpha^2\delta\epsilon^3 + 2\alpha\beta\delta^2\epsilon^3 + 2\alpha\beta\epsilon^3 + 2\alpha\delta^4\epsilon^5 + 2\alpha\delta^3\epsilon^4 - 2\alpha\delta^2\epsilon^5 - 2\alpha\epsilon^3 + 4\beta\delta\epsilon^3 + 2\beta\epsilon^2 + 4\delta^3\epsilon^5 \\ &\quad + 6\delta^2\epsilon^4 - 4\delta\epsilon^5 + 2\delta\epsilon^3 - 2\epsilon^4, \\ b_8 &= -\alpha^2\delta^2\epsilon^4 + 2\alpha\beta\delta\epsilon^4 - 2\alpha\delta\epsilon^4 - \beta^2\epsilon^4 + \beta^2\epsilon^2 + 2\beta\delta^2\epsilon^4 + 2\beta\delta\epsilon^3 + \delta^4\epsilon^6 + 2\delta^3\epsilon^5 - 2\delta^2\epsilon^6 + \delta^2\epsilon^4 \\ &\quad - 2\delta\epsilon^5 + \epsilon^6 - \epsilon^4. \end{aligned} \quad (29)$$

Numerical investigation of stability regions in the space of parameters is a necessary step due to the very complicated exact forms of stability conditions of equilibrium points. It is known that the arguments of eigenvalues of the Jacobian matrix should satisfy

$$\text{Arg}\left(\lambda_i > \frac{\xi\pi}{2}\right), \quad (30)$$

to ensure the local asymptotic stability of the equilibrium point.

Stability regions for the equilibrium point of the proposed system (7) are shown in Figure 2 for different planes of  $\epsilon - \delta$  parameters when different values of the fractional order  $\xi$  are employed such that (a)  $\xi = 0.45$ , (b)  $\xi = 0.4$ , and (c)  $\xi = 0.3$ . The other values of parameters in the system are  $\alpha = 0.4$ ,  $\beta = 1.5$ ,  $\gamma = -0.4$ , and  $\sigma = 0.3$ . In Figure 3, stability regions for the equilibrium point of the proposed system (7) are shown in different planes of  $\epsilon - \xi$  parameters for different values of  $\delta$  such that (a)  $\delta = 1$ , (b)  $\delta = 0.7$ , and (c)  $\delta = 0.5$ . The other values of parameters are taken as

$\alpha = 0.4$ ,  $\beta = 1.5$ ,  $\gamma = -0.4$ , and  $\sigma = 0.3$ . Similarly, the stability regions for the equilibrium point of system (7) are shown in Figure 4 for different planes of  $\epsilon - \gamma$  parameters at different values of the fractional order  $\xi$  such that (a)  $\xi = 0.9$ , (b)  $\xi = 0.7$ , and (c)  $\xi = 0.5$ . The other values of parameters are selected as  $\alpha = 7.82$ ,  $\beta = 7.8125$ ,  $\delta = 0.5$ , and  $\sigma = 5$ .

For the suggested system (8), stability regions for the equilibrium point of the system are illustrated in Figure 5 for different planes of  $\alpha - \gamma$  parameters for different values of the fractional order  $\xi$  such that (a)  $\xi = 0.95$ , (b)  $\xi = 0.75$ , and (c)  $\xi = 0.5$ . The other values of parameters are chosen as  $\epsilon = 0.3$ ,  $\beta = 1.3$ ,  $\delta = 0.6$ , and  $\sigma = 0.03$ . In Figure 6, stability regions for the equilibrium point of the proposed system (8) are shown in different planes of  $\epsilon - \delta$  parameters for different values of the fractional order  $\xi$  such that (a)  $\xi = 0.6$ , (b)  $\xi = 0.4$ , and (c)  $\xi = 0.3$ . The other values of parameters are  $\alpha = 3.3$ ,  $\beta = 1.3$ ,  $\gamma = -0.07$ , and  $\sigma = 0.03$ , whereas in subfigure (c),  $\beta = 1.5$  and  $\gamma = -0.4$ . Finally, the stability regions for the equilibrium point of the proposed system (8) are shown in Figure 7 for different planes of  $\epsilon - \xi$  parameters

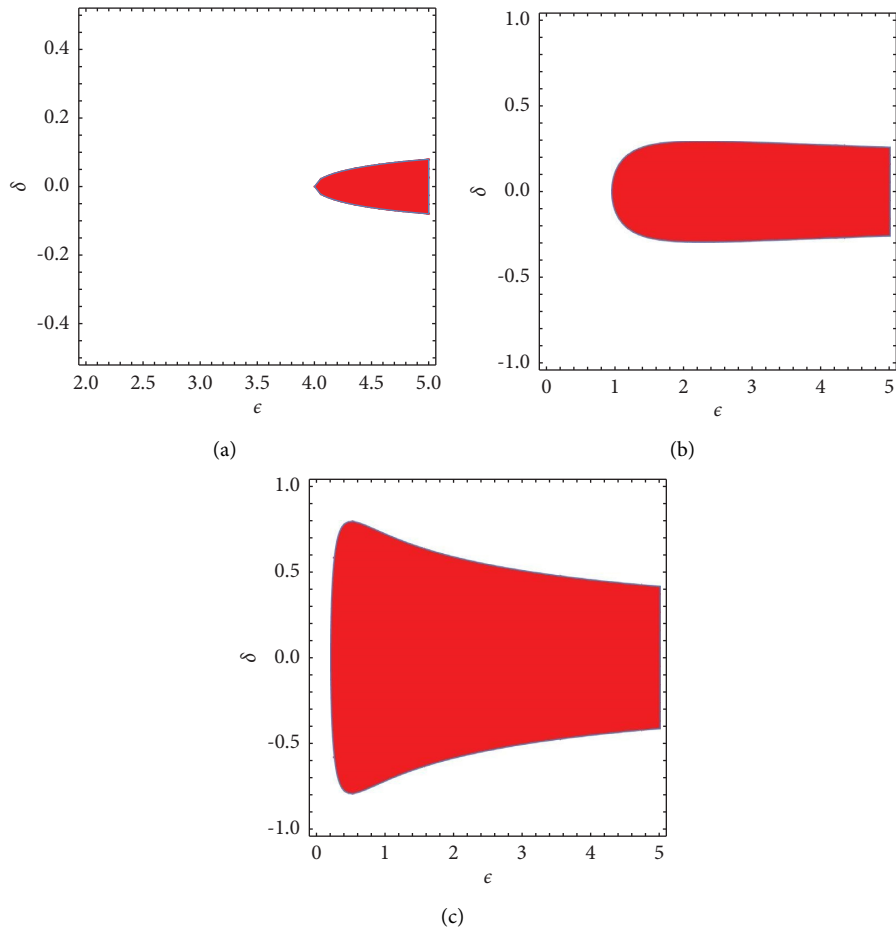


FIGURE 2: Stability regions for the equilibrium point of the proposed system (7) are shown in different planes of  $\epsilon - \delta$  parameters for different values of the fractional order  $\xi$  such that (a)  $\xi = 0.45$ , (b)  $\xi = 0.4$ , and (c)  $\xi = 0.3$ . The other values of parameters are  $\alpha = 0.4$ ,  $\beta = 1.5$ ,  $\gamma = -0.4$ , and  $\sigma = 0.3$ .

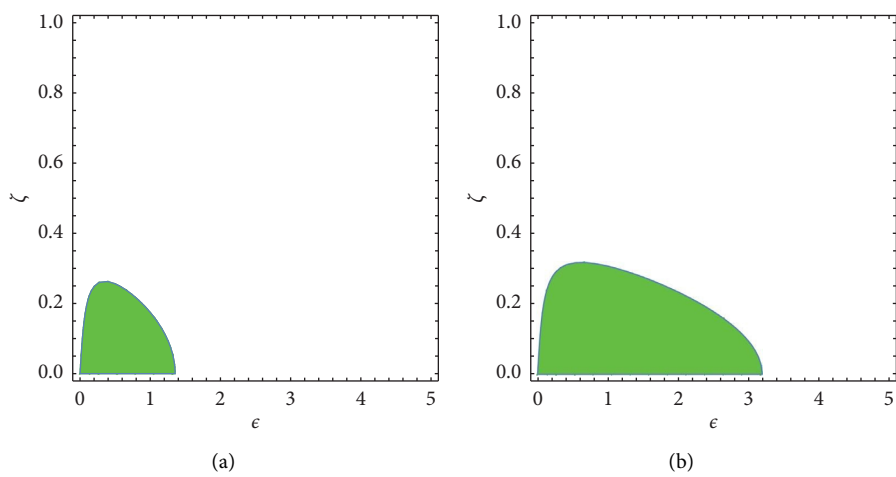


FIGURE 3: Continued.

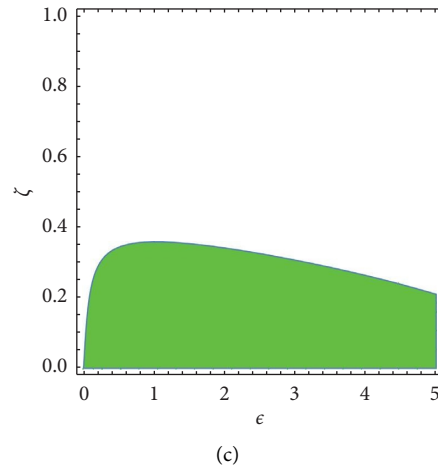


FIGURE 3: Stability regions for the equilibrium point of the proposed system (37 d phase portraits for system (7)) are shown in different planes of  $\epsilon - \xi$  parameters for different values of  $\delta$  such that (a)  $\delta = 1$ , (b)  $\delta = 0.7$ , and (c)  $\delta = 0.5$ . The other values of parameters are  $\alpha = 0.4, \beta = 1.5, \gamma = -0.4$ , and  $\sigma = 0.3$ .

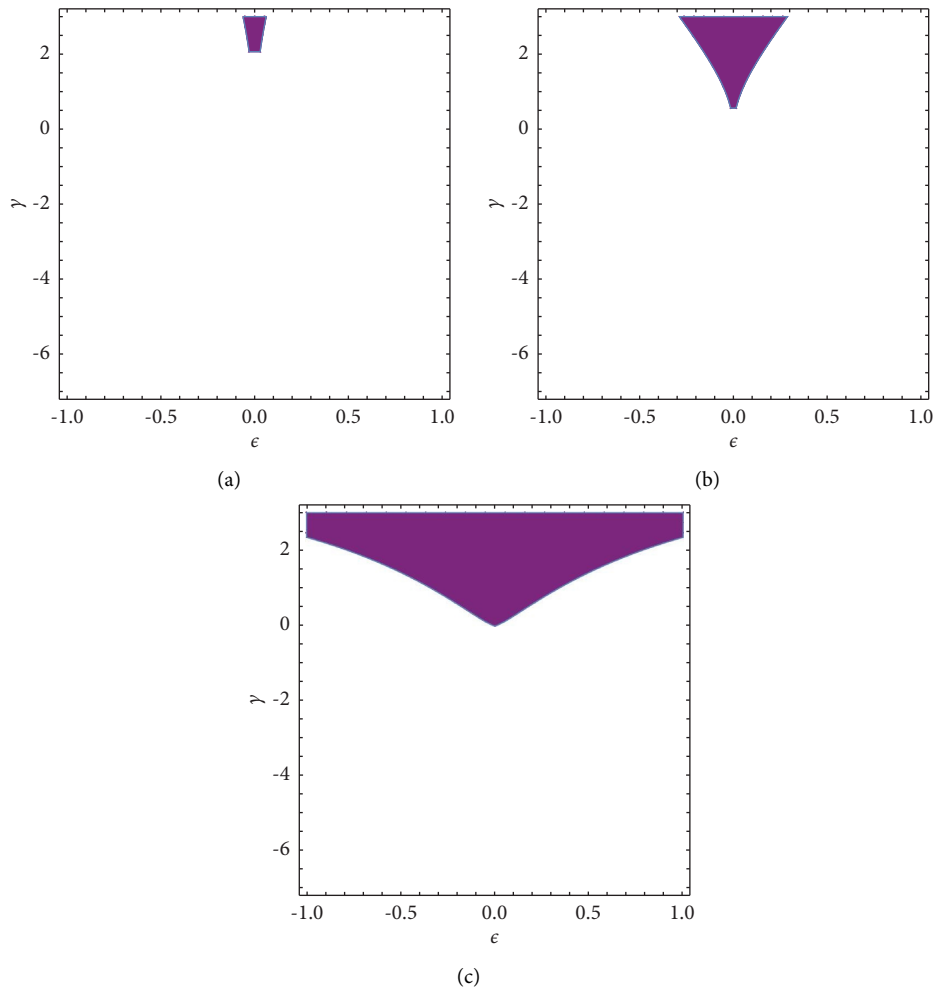


FIGURE 4: Stability regions for the equilibrium point of the proposed system (3) are shown in different planes of  $\epsilon - \gamma$  parameters for different values of the fractional order  $\xi$  such that (a)  $\xi = 0.9$ , (b)  $\xi = 0.7$ , and (c)  $\xi = 0.5$ . The other values of parameters are  $\alpha = 7.82, \beta = 7.8125, \delta = 0.5$ , and  $\sigma = 5$ .

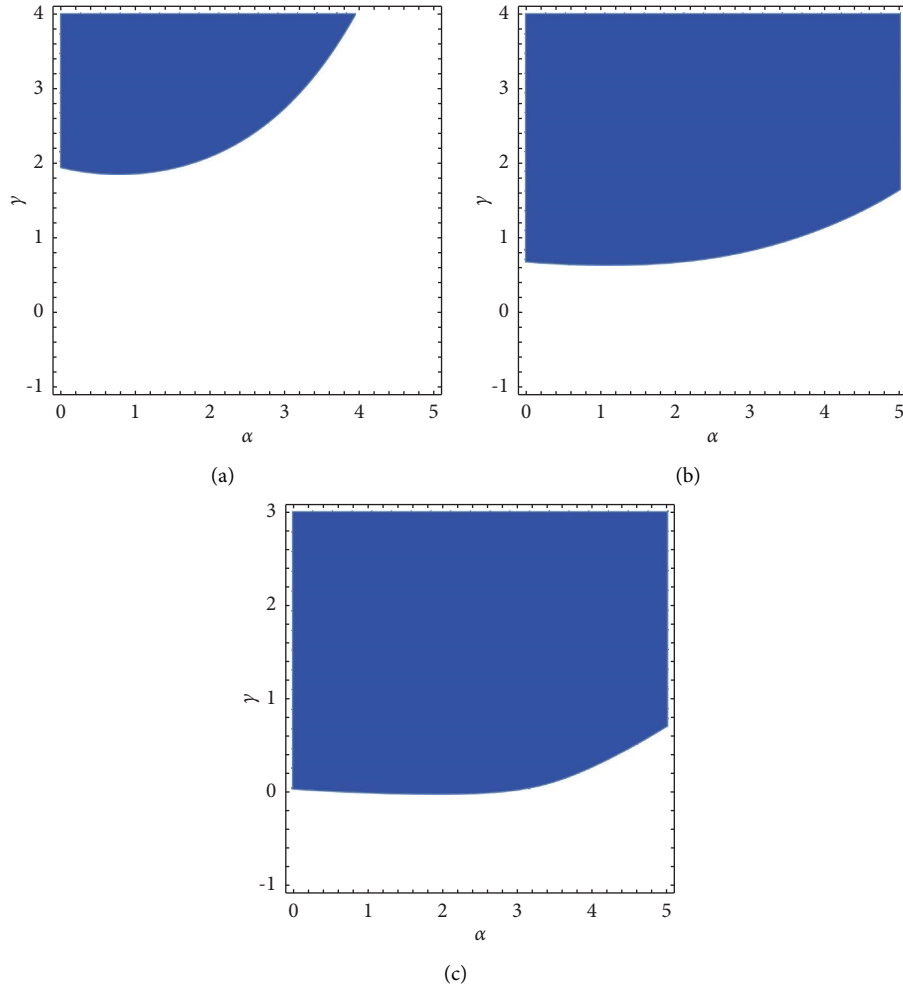


FIGURE 5: Stability regions for the equilibrium point of the proposed system (4) are shown in different planes of  $\alpha - \gamma$  parameters for different values of the fractional order  $\xi$  such that (a)  $\xi = 0.95$ , (b)  $\xi = 0.75$ , and (c)  $\xi = 0.5$ . The other values of parameters are  $\epsilon = 0.3, \beta = 1.3, \delta = 0.6$ , and  $\sigma = 0.03$ .

for different values of  $\delta$ . In particular, the following cases are considered: (a)  $\delta = 1$  and (b)  $\delta = 0.7$ , whereas the other values of parameters are taken as  $\alpha = 0.3, \beta = 1.5, \gamma = -0.4$ , and  $\sigma = 0.4$  (for case (a)) and  $\sigma = 0.3$  (for case (b)).

Numerical simulations are used to verify these obtained regions. In Figure 8, the time series plots and phase portraits for system (7) are shown at the following values of parameters  $\epsilon = 0.05, \xi = 0.7, \delta = 0.5, \alpha = 7.82, \beta = 7.813, \gamma = 2$ , and  $\sigma = 5$  and illustrate the asymptotic stability of the origin equilibrium point. Also, in Figure 9, the time series plots and phase portraits for system (48) point of the proposed system (8)) are shown at the following values of parameters  $\epsilon = 0.3, \xi = 0.9, \delta = 0.6, \alpha = 1, \beta = 1.3, \gamma = 2.8$ , and  $\sigma = 0.03$  and depict the asymptotic stability of the origin equilibrium point.

#### 4. Bifurcation Diagrams and Impact of Parameters

This section studies the impact of the following system parameters:

$$\begin{aligned}
 D^\xi x_1(t) &= -\gamma x_1 + \sigma y_1 - x_1 w_1^2 + \epsilon(w_2 - \delta x_1), \\
 D^\xi y_1(t) &= \alpha_1 x_1 - y_1 - z_1, \\
 D^\xi z_1(t) &= \beta y_1, \\
 D^\xi w_1(t) &= x_1, \\
 D^\xi x_2(t) &= -\gamma x_2 + \sigma y_2 - x_2 w_2^2 + \epsilon(-w_1 + \delta x_2), \\
 D^\xi y_2(t) &= \alpha_2 x_2 - y_2 - z_2, \\
 D^\xi z_2(t) &= \beta y_2, \\
 D^\xi w_2(t) &= x_2,
 \end{aligned} \tag{31}$$

with two different values of the parameter  $\alpha$ . Therefore, for the parameter values,  $\alpha_1 = 1.5, \alpha_2 = 12, \beta = 6, \epsilon = 2, \delta = 0.2, \sigma = 3$ , and  $\xi = 0.98$ , and initial conditions are set as  $(0.01, 0.01, 0.01, 0.2, 0.01, 0.01, 0.01, \text{ and } 0.2)$ . The parameter  $-\gamma$  varies in the range  $[-6, 10]$ , and the bifurcation diagram and corresponding Lyapunov exponents are presented in Figure 10(a). For  $-6 \leq -\gamma \leq 2.1$ , there is 2-period doubling, and for  $2.1 \leq -\gamma \leq 10$ , the system goes to chaos. When fixing

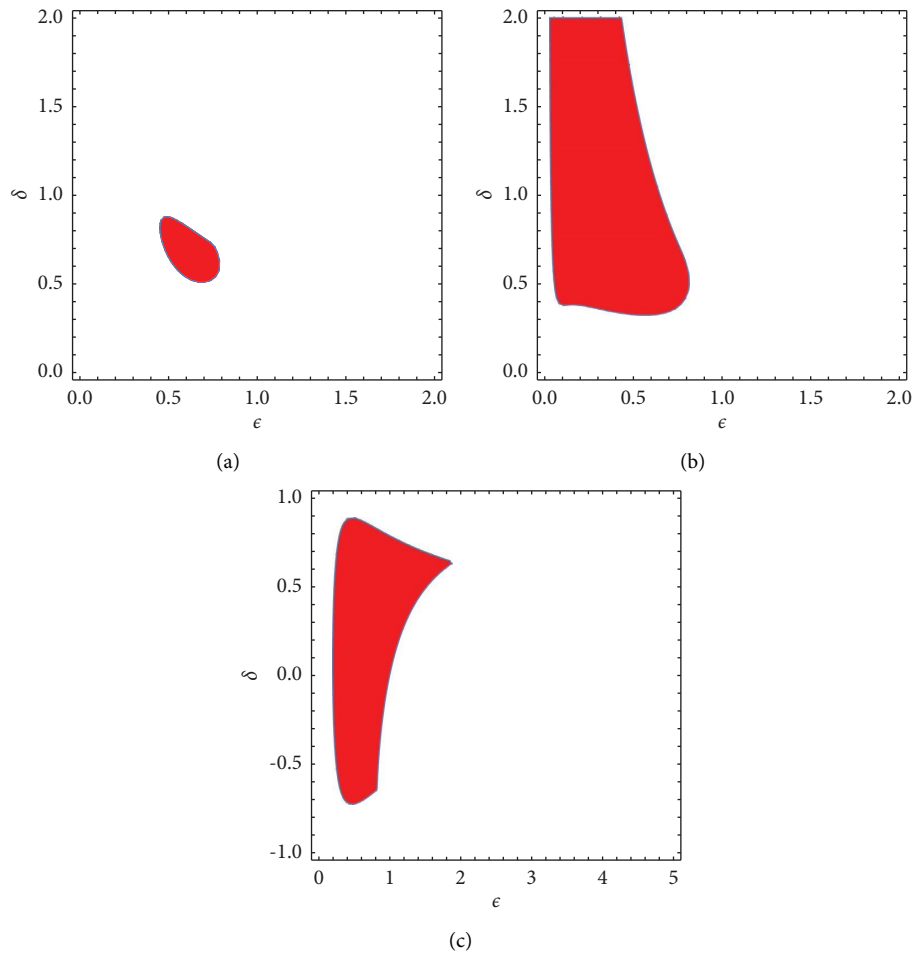


FIGURE 6: Stability regions for the equilibrium point of the proposed system (4) are shown in different planes of  $\epsilon - \delta$  parameters for different values of the fractional order  $\xi$  such that (a)  $\xi = 0.6$ , (b)  $\xi = 0.4$ , and (c)  $\xi = 0.3$ . The other values of parameters are  $\alpha = 3.3, \beta = 1.3, \gamma = -0.07$ , and  $\sigma = 0.03$ . In (c),  $\beta = 1.5$  and  $\gamma = -0.4$ .

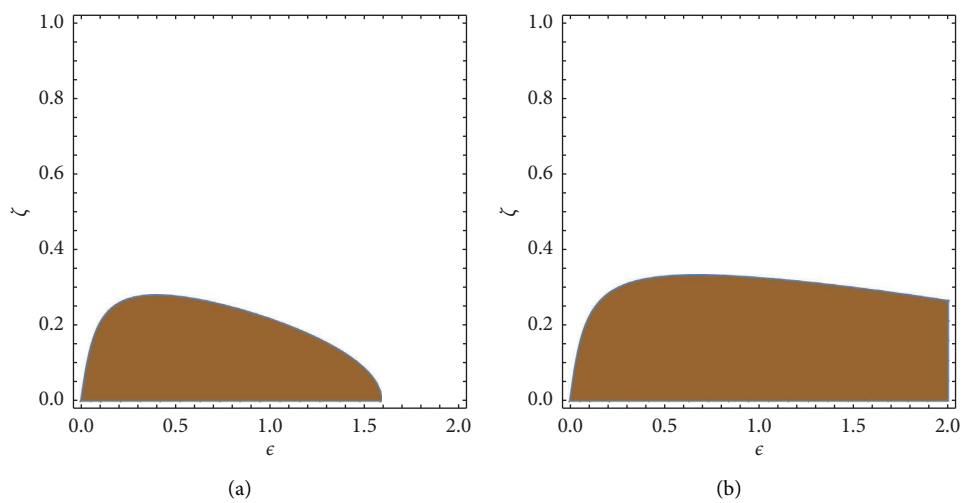


FIGURE 7: Stability regions for the equilibrium point of the proposed system (4) are shown in different planes of  $\epsilon - \xi$  parameters for different values of  $\delta$  such that (a)  $\delta = 1$  and (b)  $\delta = 0.7$ . The other values of parameters are  $\alpha = 0.3, \beta = 1.5, \gamma = -0.4$ , and  $\sigma = 0.4$ . In (b),  $\sigma = 0.3$ .

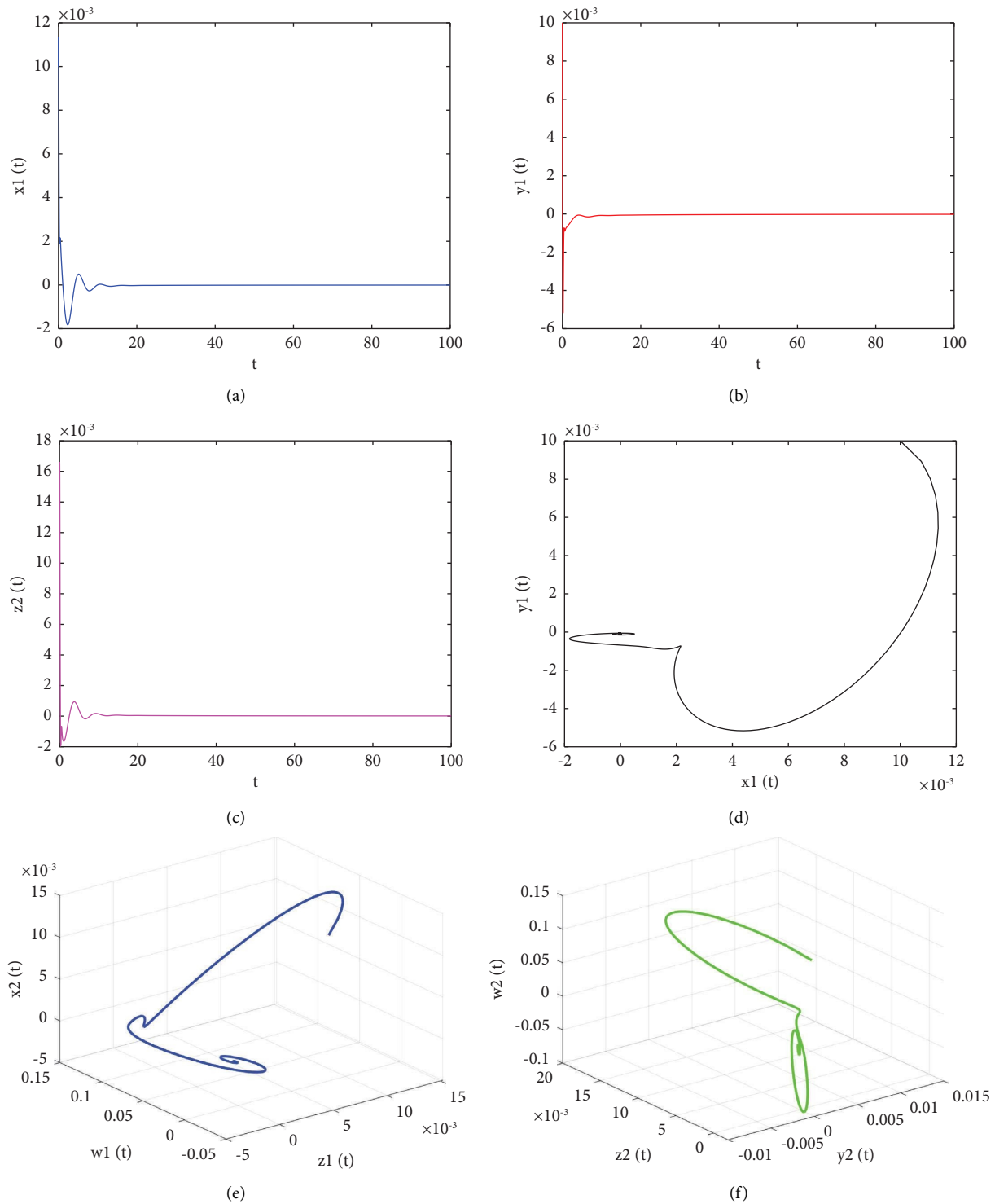


FIGURE 8: Time series plots and phase portraits for system (3) are shown at the following values of parameters  $\epsilon = 0.05, \xi = 0.7, \delta = 0.5, \alpha = 7.82, \beta = 7.813, \gamma = 2,$  and  $\sigma = 5$  and illustrate the asymptotic stability of the origin equilibrium point.

$-\gamma = 6$  and changing the value of parameter  $\alpha_1$  through the range  $[0.1, 5.5]$ , we obtain the results shown in Figure 10(b). In the interval  $[0.1, 0.8]$ , there is 6-period doubling, and the system goes to chaos and then back to period doubling in the range  $[3.5, 5.5]$ .

We fix  $\alpha_1 = 1.4$  and the varying parameter  $\beta$  in the range  $[1, 10.5]$ , as depicted in Figure 11(a). For  $1 \leq \beta \leq 3.7$  there is 2-period doubling, and then, the chaotic behavior emerges. We fix  $\beta = 5$ ; then, we examine the effect of the parameter  $\alpha_2$  through the range  $[0.1, 12.5]$ , as shown in Figure 11(b). For

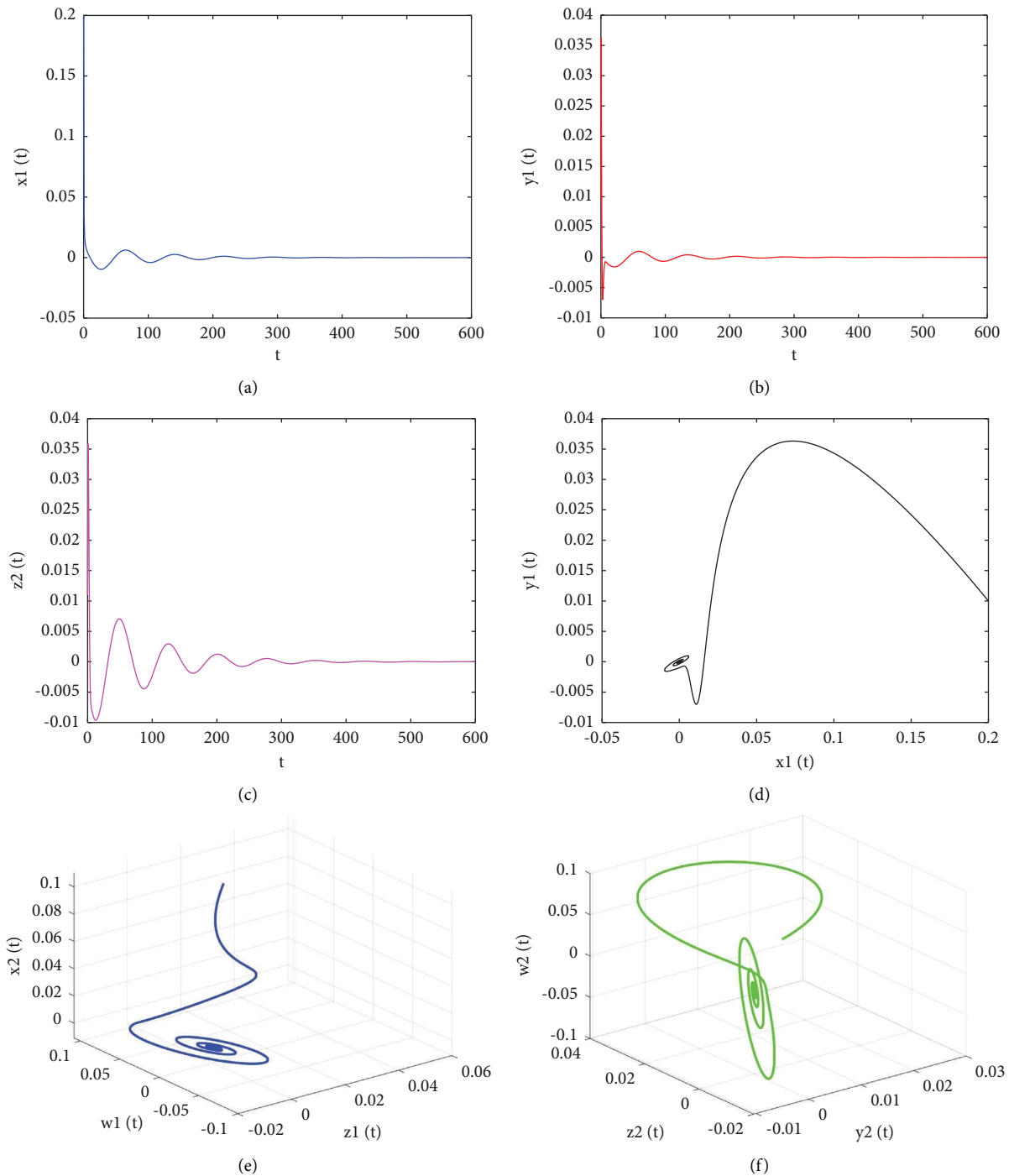


FIGURE 9: Time series plots and phase portraits for system (4) are shown at the following values of parameters  $\epsilon = 0.3$ ,  $\xi = 0.9$ ,  $\delta = 0.6$ ,  $\alpha = 1$ ,  $\beta = 1.3$ ,  $\gamma = 2.8$ , and  $\sigma = 0.03$  and illustrate the asymptotic stability of the origin equilibrium point.

$0.1 \leq \alpha_2 \leq 3.8$ , there is 3-period doubling, and for  $3.8 \leq \alpha_2 \leq 12.5$ , the system exhibits chaotic behavior.

We fix  $\alpha_2 = 6.5$ ; then, we change the value of  $\epsilon \in [0, 3]$ , as displayed in Figure 12. It is clear that, in the range  $[0, 1.2]$ , there is quasi-periodic behavior, and then, the system goes to chaos and back to 2-period doubling in  $[2.6, 3]$ . The parameter  $\epsilon$  is fixed with the value  $\epsilon = 1.5$ ; then, we change the value of parameters  $\delta \in [0, 0.99]$  and  $\delta \in [0, 10]$ , as depicted

in Figures 13(a) and 13(b), respectively. In the range of  $0 \leq \delta \leq 0.3$ , the system exhibits chaotic behavior, and then, 2-period doubling behavior appears. For the parameter  $\sigma$  in the range from  $\sigma = 0.5$  to  $\sigma = 4$ , we fix  $\delta = 0.6$ , and the bifurcation diagram and the corresponding Lyapunov exponent plot are shown in Figures 14(a) and 14(b), respectively. The figures show that, in the interval  $[0.5, 1.75]$ , the value of the maximal Lyapunov exponent is very close to



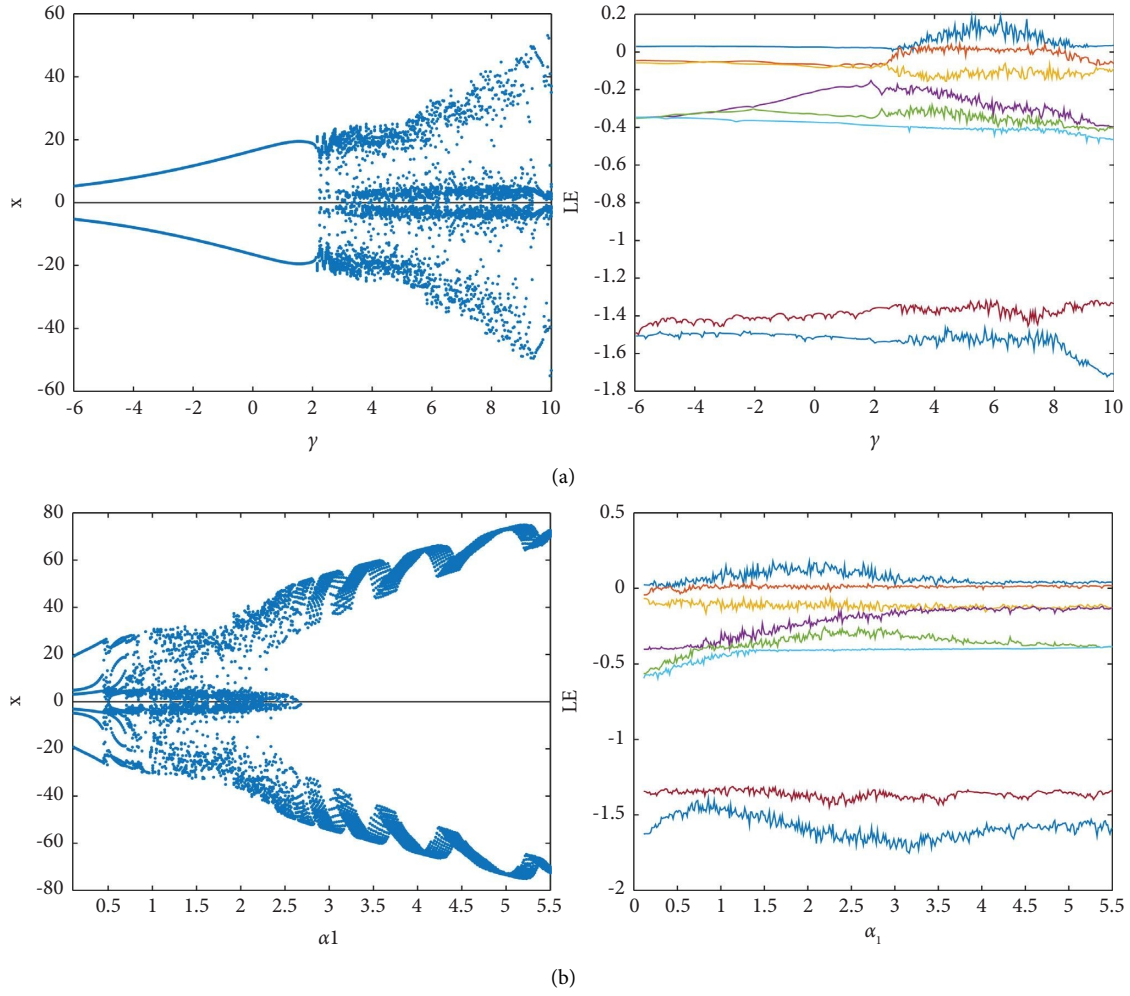


FIGURE 10: The bifurcation diagram and corresponding Lyapunov exponents for (a)  $-\gamma$  and (b)  $\alpha_1$ .

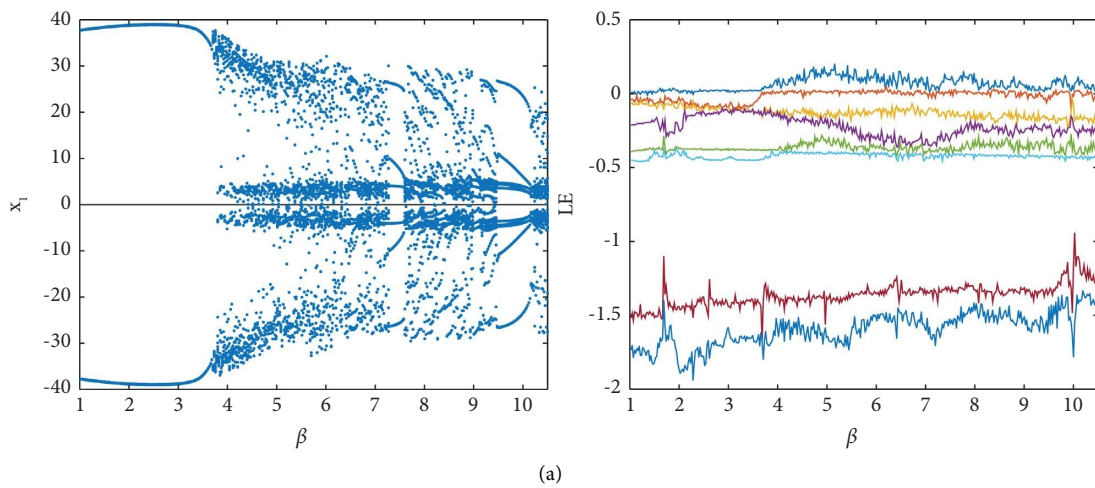


FIGURE 11: Continued.

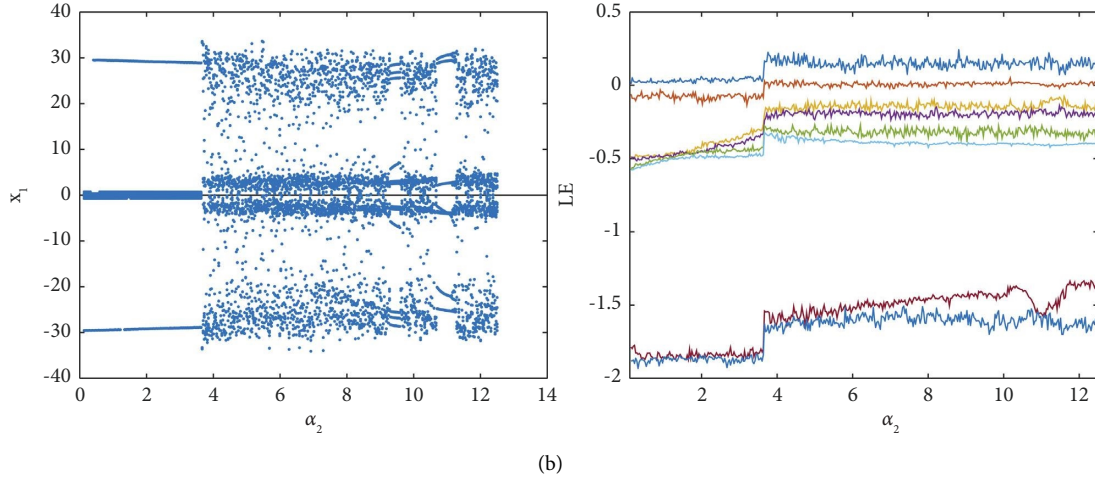


FIGURE 11: The bifurcation diagram and corresponding Lyapunov exponents for (a)  $\beta$  and (b)  $\alpha_2$ .

0, which indicates that periodic behavior occurs in this range, followed by period doubling cascade in [1.75, 2.2]. Finally, the chaotic behavior is observed in [2.2, 4].

We fix  $\beta = 3$ , and then, we change the value of the fractional order  $\xi \in [0.75, 1]$ , as displayed in Figure 15. For  $0.75 \leq \xi \leq 0.865$ , there is 2-period doubling, and then, the system goes to quasi-periodic and back to chaos. The phase portrait at two different values for the fractional order  $\xi$  is depicted in Figures 16 and 17 to verify the bifurcation diagram.

## 5. Image Encryption and the Decryption Algorithm

We are motivated by coupled fractional-order memristor chaotic systems and their sensitivity to initial conditions to utilize the generated randomness time series from the coupled system in an image encryption application. The algorithm fundamentally consists of two parts: original image pixel scrambling with the pixel value remains unchanged and image diffusion based on the chaotic time series from the coupled fractional-order memristor chaotic systems.

**5.1. Encryption Steps.** The steps of the proposed algorithm are illustrated as follows:

- (1) The original image is put as a matrix  $B_{M \times N}$  with dimensions  $M \times N$ .
- (2) The value of the constant  $B_c$  is set as a perturbation value that relies only on the original image, and it is defined as

$$B_c = \frac{1}{(M \times N)^3} \sum_{i=1}^M \sum_{j=1}^N B(i, j), \quad (32)$$

where  $B(i, j)$  is the positions of original image pixels. We use the image constant  $B_c$  as a perturbation value for one of the system parameters, for example,  $\sigma$  or  $\alpha_1$ , to make the original image

contribute to evaluating the secret key and the scrambling process.

- (3) The chaotic time series are obtained as  $x_1(i), y_1(i), z_1(i), w_1(i), x_2(i), y_2(i), z_2(i), w_2(i), i = 1, 2, \dots, k$ , and  $k = M \times N$ ; after eliminating the transient values, the required size  $k$  is obtained from the solutions of the chaotic system.
- (4) The standard values for the secret key and new pixel positions are obtained as follows:

$$\begin{aligned} \text{secretKey}_i &= \text{mod}(\text{floor}(x_1(i) \times 10^{15}), 256), \\ \text{newRow}_i &= \text{mod}(\text{floor}(x_2(i) \times 10^{15}), M) + 1, \\ \text{newCol}_i &= \text{mod}(\text{floor}(y_2(i) \times 10^{15}), N) + 1. \end{aligned} \quad (33)$$

For the secret key, we use the mod function between  $x_1(i)$  and 256, where the range [0, 256] indicates image pixel values. Also, we use the mod function between  $x_2(i), y_2(i)$  and  $M$  and  $N$ , respectively, to get a new position for the pixel value image matrix  $B$  for the scrambling process.

- (5) The repositioned image matrix  $B_{sc}$  is obtained after using  $\text{newRow}$  and  $\text{newCol}$  as new rows and columns for pixel positions without altering pixel values.
- (6) The secret key is transformed to the matrix using

$$\text{sKey} = \text{reshape}(\text{secretKey}, M, N). \quad (34)$$

Step 7. To obtain the encrypted image  $B_{en}$ , the bitwise XOR operation between  $\text{sKey}$  and  $B_{sc}$  is applied:

$$B_{en}(i, j) = B_{sc}(i, j) \oplus \text{sKey}(i, j). \quad (35)$$

**5.2. Decryption Steps.** To decode the image, we reverse the encryption steps as follows:

Step 1. To obtain the decrypted image  $B_{de}$ , the bitwise XOR operation between  $B_{en}$  and  $\text{sKey}$  is applied:

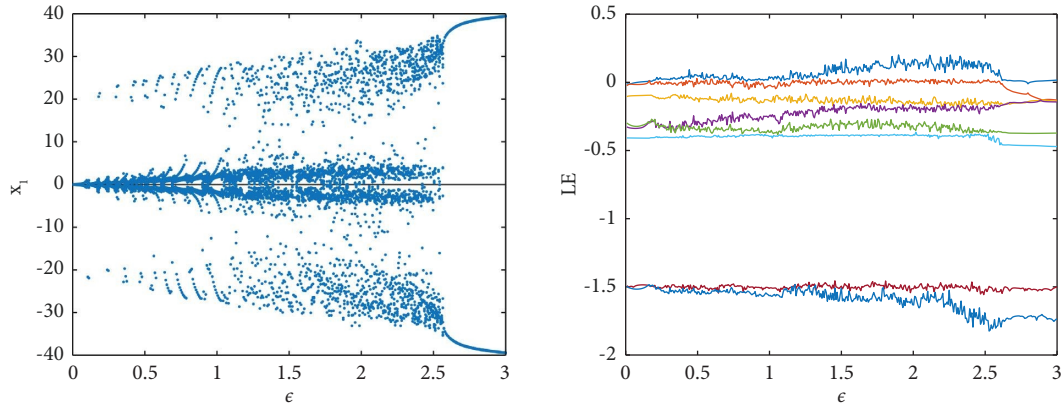


FIGURE 12: The bifurcation diagram and corresponding Lyapunov exponents for  $\epsilon$ .

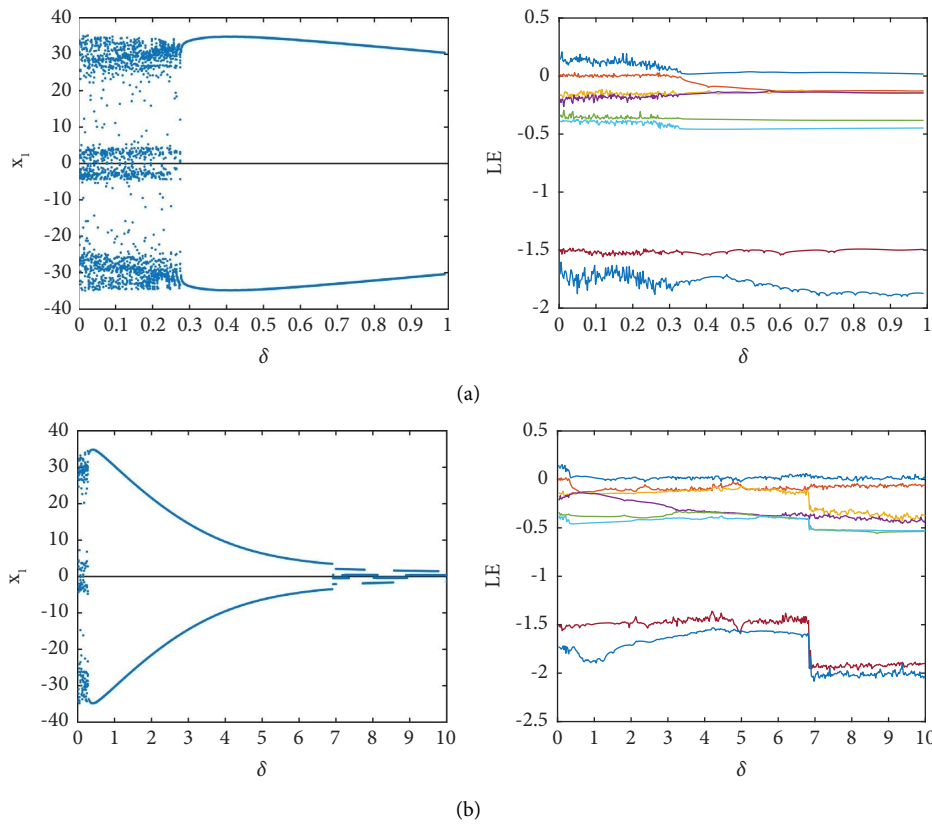


FIGURE 13: The bifurcation diagram and corresponding Lyapunov exponents for  $\delta$ . (a)  $\delta \in [0, 0.99]$  and (b)  $\delta \in [0, 10]$ .

$$B_{de}(i, j) = B_{en}(i, j) \oplus sKey(i, j). \quad (36)$$

Step 2. The positions of the pixels in the image are inverted to get the original image using newRow and newCol sequences.

5.3. Security Analysis. The encryption algorithm of images is applied based on the coupled fractional-order memristor chaotic systems. Four test images, cameraman, Lena, bird, and baboon, with a size of  $256 \times 256$  are used in the experiment. The perturbation value  $B_c$  of the cameraman,

Lena, bird, and baboon images in the algorithm through (32) is  $2.7641 \times 10^{-8}$ ,  $2.8891 \times 10^{-8}$ ,  $1.6707 \times 10^{-8}$ , and  $1.5513 \times 10^{-8}$ , respectively. The proposed encryption algorithm is implemented on the four test images, as illustrated in Figure 18 which depicts the original, scrambled, encrypted, and decrypted images for the presented algorithm.

To confirm the effectiveness of the proposed algorithm, statistical and randomness tests have been carried out such as key space, histogram analysis, information entropy, correlation coefficients of adjacent pixels, key sensitivity, and cropping attacks.

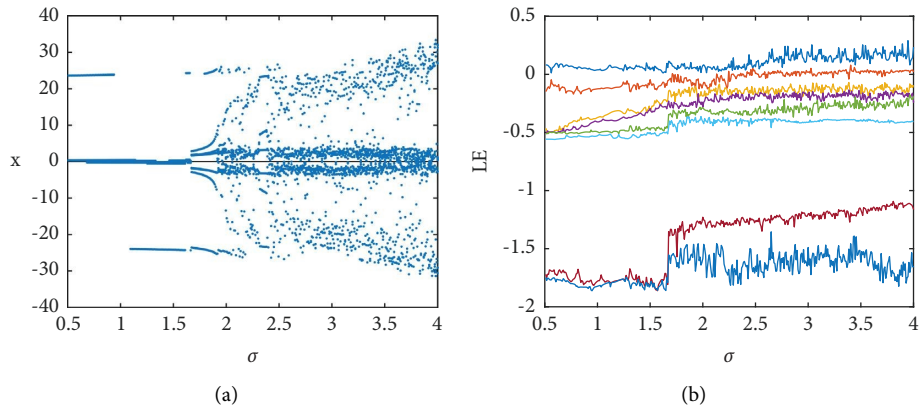


FIGURE 14: The bifurcation diagram and corresponding Lyapunov exponents for the fractional order  $\sigma$ .

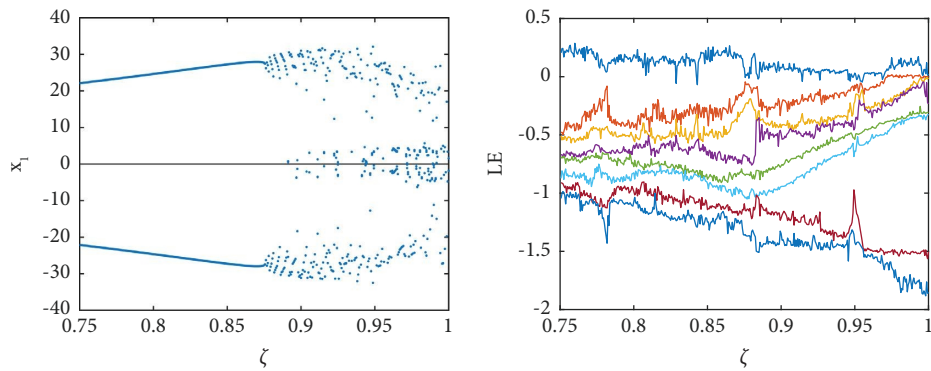


FIGURE 15: The bifurcation diagram and corresponding Lyapunov exponents for the fractional order  $\xi$ .

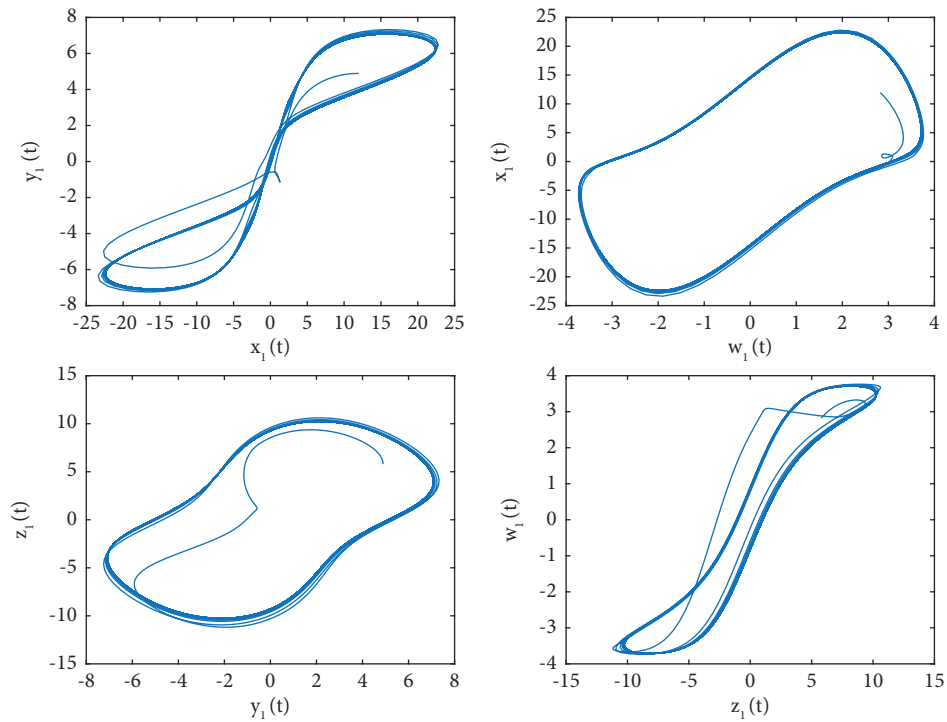


FIGURE 16: The system phase portrait at the fractional order  $\xi = 0.76$ .

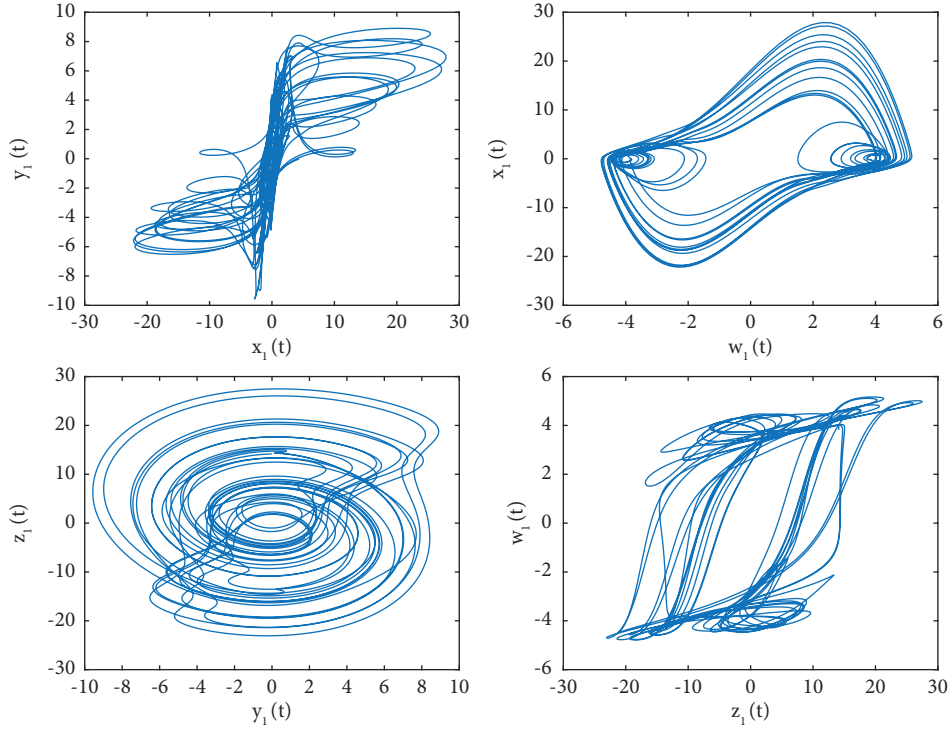


FIGURE 17: The system phase portrait at the fractional order  $\xi = 0.98$ .

5.3.1. *Key Space.* The key space refers to the key size range, which can determine the security of the encryption algorithm which is resistant to brute force attacks. In this paper, the secret key is composed of the double precision based on the chaotic coupled system parameters  $\alpha_1, \alpha_2, \beta, \epsilon, \delta, \sigma, \xi, B_c$  and initial conditions  $(x_1(0), y_1(0), z_1(0), w_1(0), x_2(0), y_2(0), z_2(0), w_2(0))$ . The digit numbers are to be at least  $10^{-15}$  in each parameter. The proposed algorithm has a key space value of  $10^{240}$  which is compared to the recommended key space that should be at least  $2^{100}$  [61]. Consequently, the large key space of the proposed algorithm provides resistance to various types of attacks.

5.3.2. *Histogram Analysis.* The histogram is an indicator of statistics in the image, which reflects the total number of pixels for each value in the image. To deny an adversary from obtaining statistical information, the histogram of the encrypted image should be uniformly distributed. For the proposed algorithm, the histogram of the original and encrypted images is shown in Figure 19, demonstrating that the encrypted image has a uniform histogram regardless of the original image; hence, it can resist statistical analysis attacks.

Moreover, the histogram variance can be used to quantify the histogram. The smaller the variance of the encrypted image, the more uniform the distribution. The histogram variances for the original and encrypted images are shown in Table 1. In all the cases, the significant reduction of the variance can be observed compared with the original image. The reduction for the cameraman, Lena, bird

and baboon images is verified with values of approximately 99%.

5.3.3. *Information Entropy.* Information entropy is a tool used to measure the randomness of pixels in an image. The values of entropy are 7.9978, 7.9971, 7.9974, and 7.9973 for cameraman, Lena, bird, and baboon images, respectively. It is clear that the mentioned values approach the ideal value  $\approx 8$ , which means that the encrypted image has high randomness and is less feasible to show information for the encryption scheme. In Table 2, the entropy of the proposed algorithm is compared with the similar literature work.

5.3.4. *Correlation Analysis.* The correlation analysis is used to represent the degree of association between adjacent pixels, and the correlation coefficient is close to 1 in the original image. The calculation method of the correlation coefficient between adjacent pixels is as follows:

$$r_{uv} = \frac{\text{cov}(u, v)}{\sqrt{\sigma_u \sigma_v}}, \quad (37)$$

where  $\text{cov}(u, v)$  is the covariance function,  $E(u) = 1/N \sum_{i=1}^N u_i$ , and  $\sigma_u = 1/N \sum_{i=1}^N (u_i - E(u))^2$ . The correlation analysis of the cameraman, Lena, bird, and baboon original and encrypted images in three directions is evaluated and shown in Table 3. In addition, the correlations of the bird image before and after encryption in each direction are depicted in Figure 20. It is clear that the correlation coefficient of the encrypted image is close to zero in all directions. Therefore, the encryption process



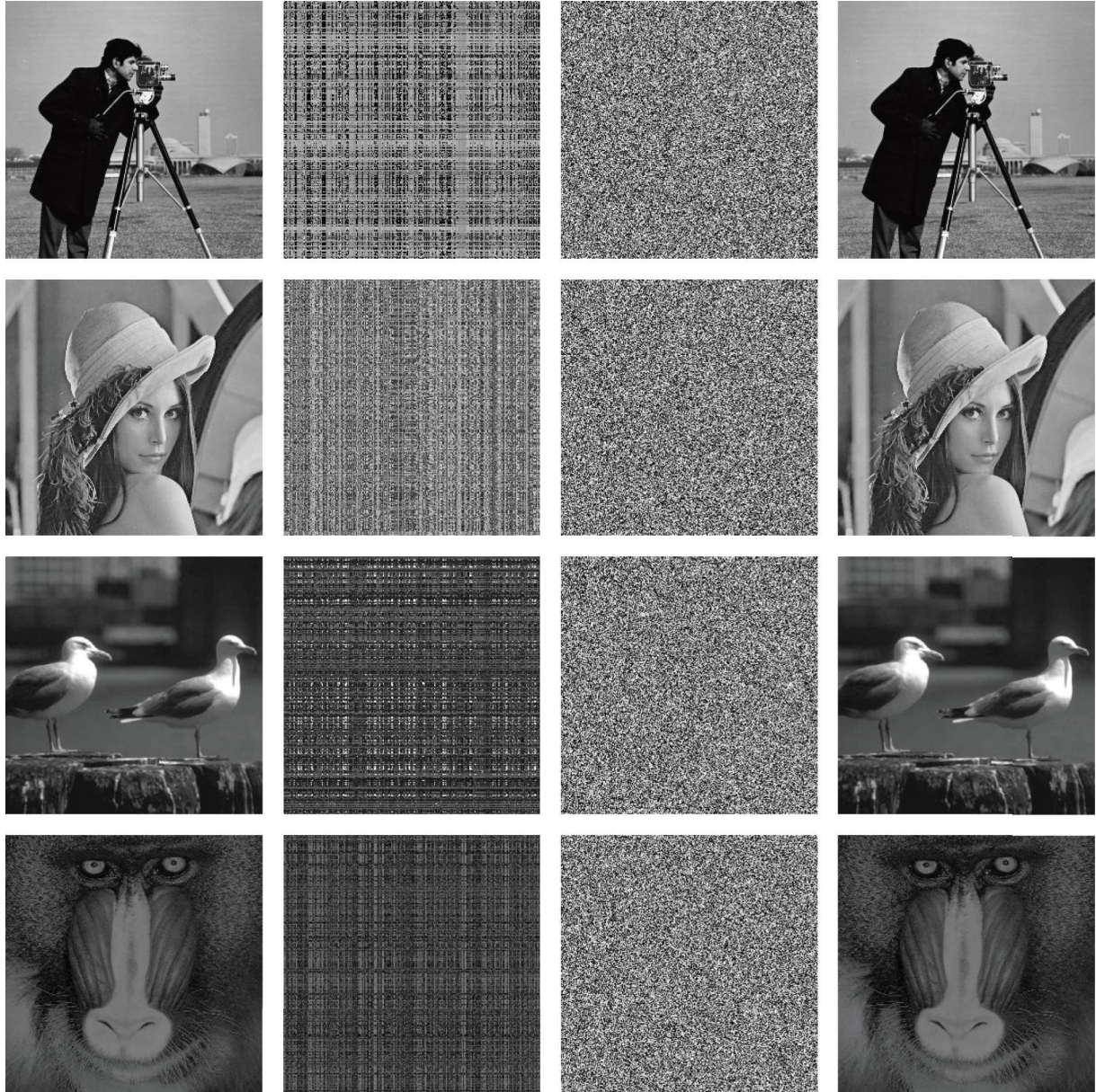


FIGURE 18: The original, shuffled, encrypted, and decrypted images in first, second, third, and fourth columns, respectively, for cameraman, Lena, bird, and baboon images with a size of  $256 \times 256$ .

makes pixels of the encrypted image almost independent of each other. Consequently, the encryption algorithm breaks the original statistical features of the data of the original image.

**5.3.5. Key Sensitivity Analysis.** The encryption algorithm should be very sensitive to its secret key. Therefore, a slight change in the key will lead to a complete change in the encryption result. Hence, if the secret key changes slightly, the decrypted image will be different from the original image. To measure the sensitivity of the encryption key, NPCR (pixel change rate) and UACI (pixel average change intensity) have been used. NPCR and UACI are evaluated by the following equations [65]:

$$\text{NPCR}(\%) = \frac{\sum_{i=1}^M \sum_{j=1}^N |\text{sign}(P_1(i, j) - P_2(i, j))|}{M \times N} \times 100,$$

$$\text{UACI}(\%) = \frac{1}{M \times N} \sum_{i=1}^M \sum_{j=1}^N \frac{|P_1(i, j) - P_2(i, j)|}{255} \times 100. \quad (38)$$

We verified the sensitivity of secret key values associated with  $x_1(0)$  and  $y_1(0)$  by adding  $10^{-12}$  in the initial conditions. The values of NPCR and UACI between the encrypted image and the original image are evaluated in Table 4. It can be confirmed that the proposed algorithm has a good sensitivity to the encryption key.

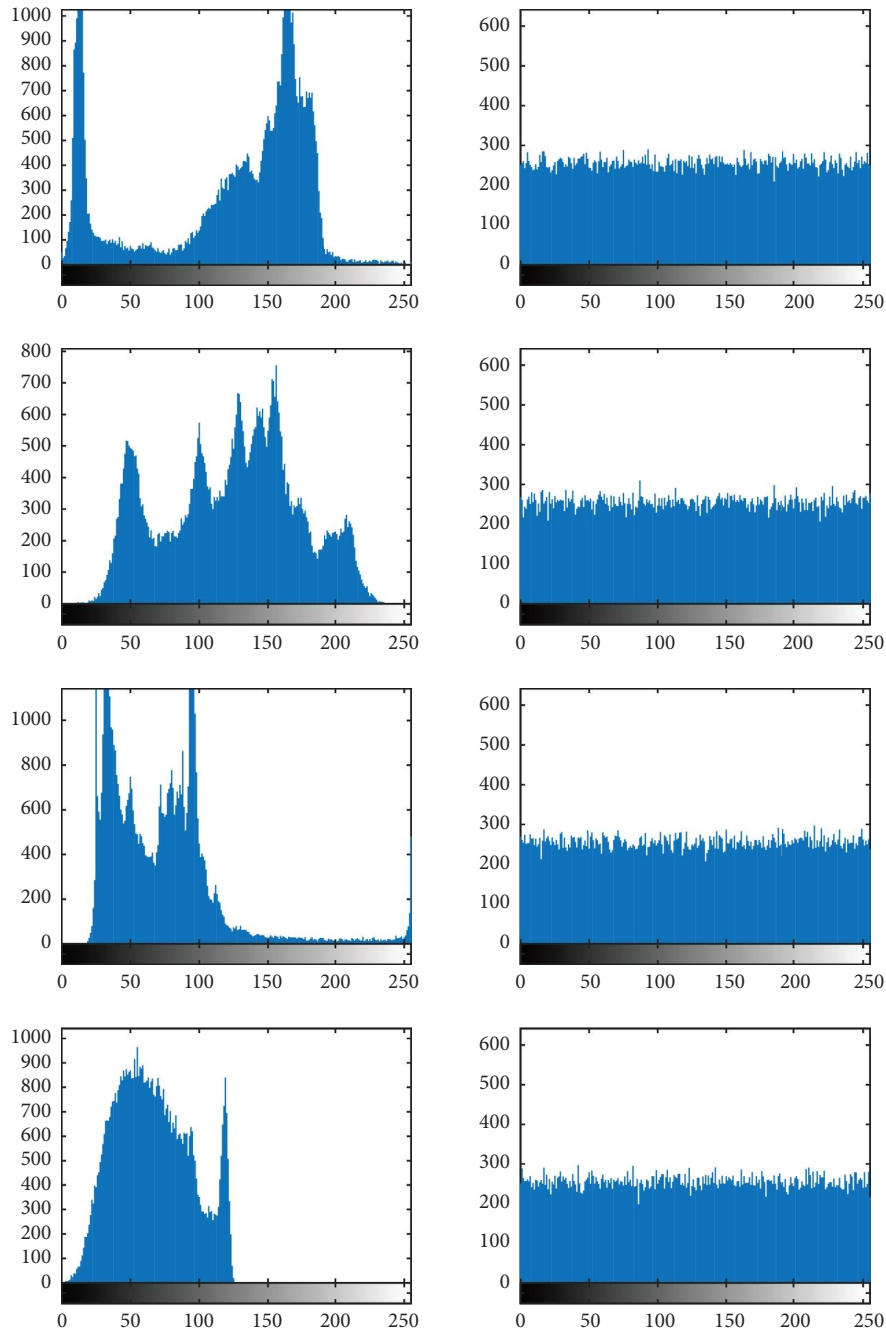


FIGURE 19: Histograms for cameraman, Lena, bird, and baboon images in the first, second, and third rows, respectively. First column: original images; second column: encrypted images.

TABLE 1: The histogram variances for original and encrypted images for cameraman, Lena, bird, and baboon images with their reduction.

	Original	Encrypted	Reduction (%)
Cameraman	102940	203.3176	99.8025
Lena	39104	259.3961	99.3366
Bird	143930	238.3922	99.8344
Baboon	107900	247.098	99.771

5.3.6. *Cropping Attack.* To investigate the immunity of the encryption algorithm to some information loss or tampered information, the cropping attack is utilized. In the proposed

algorithm, we can still obtain an identifiable image by decryption when an internal block of the encrypted image with a dimension of  $256 \times 75$  is exchanged with a black block in



TABLE 2: Comparison of the entropy of the proposed algorithm with the literature.

Images	Proposed	Ref. [62]	Ref. [63]	Ref. [64]
Cameraman	7.9978	—	—	7.9661
Lena	7.9971	7.9976	7.997	7.9661
Baboon	7.9973	7.9972	7.997	—

TABLE 3: The correlation coefficients of the four images in different directions.

Image		Horizontal	Vertical	Diagonal
Cameraman	Original	0.9331	0.9583	0.9080
	Encrypted	-0.0067	-0.0044	-0.0024
Lena	Original	0.9046	0.9443	0.8835
	Encrypted	0.0019	-0.0015	-0.0039
Bird	Original	0.9748	0.9634	0.9483
	Encrypted	-0.0020	0.0061	0.0007
Baboon	Original	0.8623	0.8184	0.8090
	Encrypted	0.0004	-0.0087	0.0031

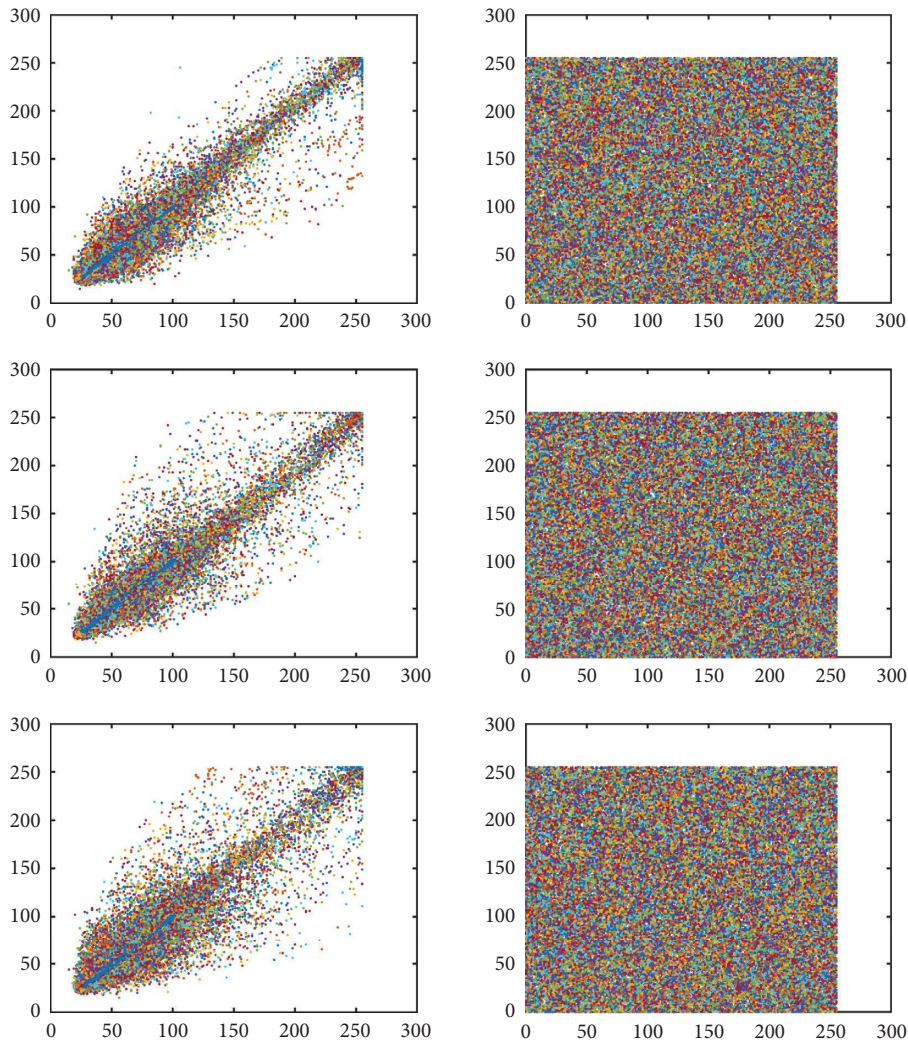


FIGURE 20: The correlation of the bird original image in the first column and the encrypted image in the second column for the three directions.



TABLE 4: The values of NPCR (%) and UACI (%) results for the cameraman, Lena, bird, and baboon images.

Image	NPCR (%)	UACI (%)
Cameraman	99.5575	33.4745
Lena	99.5728	33.4263
Bird	99.5911	33.5066
Baboon	99.6033	33.3090

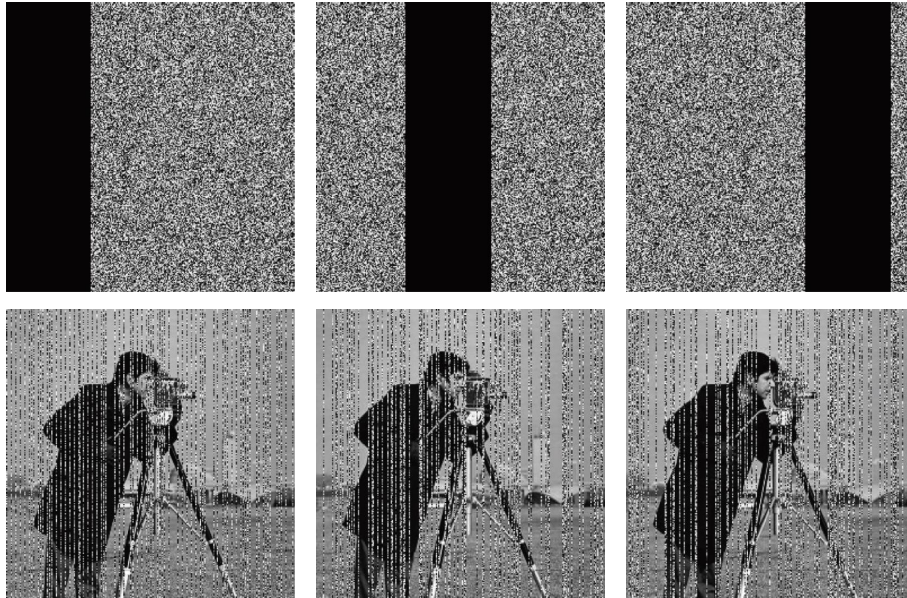


FIGURE 21: The first and second rows represent the encrypted images and the respective decrypted images as a result of the cropping attack, respectively.

different positions like left, middle, and right, as displayed in Figure 21. This illustrates that the proposed algorithm has a good ability to resist cropping and tampering attacks.

## 6. Conclusion

In this study, two coupling schemes for fractional-order memristor-based chaotic circuits are introduced. It is observed that the line of nonisolated equilibrium points in uncoupled circuits becomes a unique equilibrium point in the two coupled cases. The regions of stability in the space of parameters are depicted for each coupled system. The variety of nonlinear dynamics exhibited by the coupled circuits is examined via bifurcation diagrams, Lyapunov exponents, and phase portraits. A suggested chaos-based encryption scheme is presented. Security tests and analysis are carried out to confirm reliability of the encryption scheme.

This work is limited to the case of two coupled fractional-order chaotic circuits. The work can be extended to the more realistic and general cases of coupled memristor-based circuits. In particular, different topologies for networks of coupled circuits can be considered in future studies. For example, it is interesting to explore the nonlinear dynamics and chaos synchronization in ring, starhub, tree, or hierarchical networks of fractional memristor-based chaotic circuits. Moreover, new chaos-based encryption schemes can be examined in different configurations of fractional circuit networks.

## Data Availability

No data were used to support the findings of this study.

## Conflicts of Interest

The authors declare that they have no conflicts of interest.

## Acknowledgments

The authors extend their appreciation to the Deputyship for Research & Innovation, Ministry of Education in Saudi Arabia for funding this research work through the project number (IF-PSAU-2021/01/18214).

## References

- [1] P. N. V. Tu, *Dynamical Systems: An Introduction with Applications in Economics and Biology*, Springer Science & Business Media, Berlin, Germany, 2012.
- [2] S. H. Strogatz, *Nonlinear Dynamics and Chaos: With Applications to Physics, Biology, Chemistry, and Engineering*, CRC Press, Florida, FL, USA, 2018.
- [3] C. H. Wang, H. Xu, and F. Yu, "A novel approach for constructing high-order Chua circuit with multi-directional multi-scroll chaotic attractors," *International Journal of Bifurcation and Chaos*, vol. 23, no. 02, Article ID 1350022, 2013.

- [4] N. Yujun, W. Xingyuan, W. Mingjun, and Z. Huaguang, "A new hyperchaotic system and its circuit implementation," *Communications in Nonlinear Science and Numerical Simulation*, vol. 15, no. 11, pp. 3518–3524, 2010.
- [5] A. S. Hegazi, E. Ahmed, and A. E. Matouk, "On chaos control and synchronization of the commensurate fractional order Liu system," *Communications in Nonlinear Science and Numerical Simulation*, vol. 18, no. 5, pp. 1193–1202, 2013.
- [6] Y. Chai, L. Chen, R. Wu, and J. Dai, "Q-S synchronization of the fractional-order unified system," *Pramana*, vol. 80, no. 3, pp. 449–461, 2013.
- [7] G. Chen and X. Yu, *Chaos Control- Theory and Applications*, Springer, Berlin, Germany, 2003.
- [8] S. Boccaletti, J. Kurths, G. Osipov, D. Valladares, and C. Zhou, "The synchronization of chaotic systems," *Physics Reports*, vol. 366, no. 1-2, pp. 1–101, 2002.
- [9] C. Zhu, "A novel image encryption scheme based on improved hyperchaotic sequences," *Optics Communications*, vol. 285, no. 1, pp. 29–37, 2012.
- [10] P. Stavroulakis, *Chaos Applications in Telecommunications*, CRC Press, Florida, FL, USA, 2006.
- [11] L. Kocarev and S. Lian, *Chaos-Based Cryptography*, Springer, Berlin, Germany, 2011.
- [12] E. M. Izhikevich, *Dynamical Systems in Neuroscience: The Geometry of Excitability and Bursting*, MIT Press, Cambridge, CA, USA, 2007.
- [13] T. Matsumoto, "A chaotic attractor from Chua's circuit," *IEEE Transactions on Circuits and Systems*, vol. 31, no. 12, pp. 1055–1058, 1984.
- [14] M. Shinriki, M. Yamamoto, and S. Mori, "Multi-mode oscillations in a modified van der Pol oscillator containing a positive nonlinear conductance," *Proceedings of the IEEE*, vol. 69, no. 3, pp. 394–395, 1981.
- [15] G. P. King and S. T. Gaito, "Bistable chaos. I. Unfolding the cusp," *Physical Review A*, vol. 46, no. 6, pp. 3092–3099, 1992.
- [16] A. E. Matouk and H. N. Agiza, "Bifurcations, chaos and synchronization in ADVP circuit with parallel resistor," *Journal of Mathematical Analysis and Applications*, vol. 341, no. 1, pp. 259–269, 2008.
- [17] L. O. Chua, "Memristor – the missing circuit element," *IEEE Transactions on Circuit Theory*, vol. 18, no. 5, pp. 507–519, 1971.
- [18] D. B. Strukov, G. S. Snider, D. R. Stewart, and R. S. Williams, "The missing memristor found," *Nature*, vol. 453, no. 7191, pp. 80–83, 2008.
- [19] B. Muthuswamy and P. Kokate, "Memristor based chaotic circuits," *IETE Technical Review*, vol. 26, no. 6, pp. 417–516, 2009.
- [20] P. K. Roy and A. A. Basuray, "A high frequency chaotic signal generator: a demonstration experiment," *American Journal of Physics*, vol. 71, no. 1, pp. 34–37, 2003.
- [21] K. S. Sudheer and M. Sabir, "Adaptive function projective synchronization of two-cell quantum-CNN chaotic oscillators with uncertain parameters," *Physics Letters A*, vol. 373, no. 21, pp. 1847–1851, 2009.
- [22] G. Peng and F. Min, "Multistability analysis, circuit implementations and application in image encryption of a novel memristive chaotic circuit," *Nonlinear Dynamics*, vol. 90, no. 3, pp. 1607–1625, 2017.
- [23] S. S. Arshad, A. Ali, A. Eleyan, S. A. Shah, and J. Ahmed, "Chaos theory and its application: an essential framework for image encryption," *Chaos Theory and Applications*, vol. 2, no. 1, pp. 17–22, 2020.
- [24] B. Fernandez-Carreón, J. M. Muñoz-Pacheco, E. Zambrano-Serrano, and O. G. Felix-Beltrán, "Analysis of a fractional-order glucose-insulin biological system with time delay," *Chaos Theory and Applications*, vol. 4, no. 1, pp. 10–18, 2022.
- [25] Ö. F. Boyraz, M. E. Cimen, E. Guleryuz, and M. Z. Yildiz, "A chaos-based encryption application for wrist vein images," *Chaos Theory and Applications*, vol. 3, no. 1, pp. 3–10, 2021.
- [26] A. Kilbas, H. Srivastava, and J. Trujillo, *Theory and Application of Fractional Differential Equations*, Elsevier, New York, NY, USA, 2006.
- [27] A. Al-khedhairi, A. Elsadany, and A. Elsonbaty, "Modelling immune systems based on Atangana–Baleanu fractional derivative," *Chaos, Solitons & Fractals*, vol. 129, pp. 25–39, 2019.
- [28] H. L. Li, L. Zhang, C. Hu, Y. L. Jiang, and Z. Teng, "Dynamical analysis of a fractional-order predator-prey model incorporating a prey refuge," *International Journal of Applied Mathematics and Computer Science*, vol. 54, no. 1-2, pp. 435–449, 2016.
- [29] A. Yousefpour, H. Jahanshahi, J. M. Muñoz-Pacheco, S. Bekiros, and Z. Wei, "A fractional-order hyper-chaotic economic system with transient chaos," *Chaos, Solitons & Fractals*, vol. 130, Article ID 109400, 2020.
- [30] M. A. Khan, M. A. Khan, M. Azizah, Windarto, and S. Ullah, "A fractional model for the dynamics of competition between commercial and rural banks in Indonesia," *Chaos, Solitons & Fractals*, vol. 122, pp. 32–46, 2019.
- [31] M. Wang, X. Liao, Y. Deng, Z. Li, Y. Su, and Y. Zeng, "Dynamics, synchronization and circuit implementation of a simple fractional-order chaotic system with hidden attractors," *Chaos, Solitons & Fractals*, vol. 130, Article ID 109406, 2020.
- [32] G. Si, L. Diao, and J. Zhu, "Fractional-order charge-controlled memristor: theoretical analysis and simulation," *Nonlinear Dynamics*, vol. 87, no. 4, pp. 2625–2634, 2017.
- [33] L. J. Sheu, H. K. Chen, J. H. Chen, and L. M. Tam, "Chaos in a new system with fractional order," *Chaos, Solitons & Fractals*, vol. 31, no. 5, pp. 1203–1212, 2007.
- [34] S. Pang and Y. Liu, "A new hyperchaotic system from the Lü system and its control," *Journal of Computational and Applied Mathematics*, vol. 235, no. 8, pp. 2775–2789, 2011.
- [35] Y. Yu, H. X. Li, S. Wang, and J. Yu, "Dynamic analysis of a fractional-order Lorenz chaotic system," *Chaos, Solitons & Fractals*, vol. 42, no. 2, pp. 1181–1189, 2009.
- [36] X. Chai, X. Fu, Z. Gan, Y. Lu, and Y. Chen, "A color image cryptosystem based on dynamic DNA encryption and chaos," *Signal Processing*, vol. 155, pp. 44–62, 2019.
- [37] S. Wang, C. Wang, and C. Xu, "An image encryption algorithm based on a hidden attractor chaos system and the Knuth–Durstenfeld algorithm," *Optics and Lasers in Engineering*, vol. 128, Article ID 105995, 2020.
- [38] M. Zhou and C. Wang, "A novel image encryption scheme based on conservative hyperchaotic system and closed-loop diffusion between blocks," *Signal Processing*, vol. 171, Article ID 107484, 2020.
- [39] A. Roy, A. Misra, and S. Banerjee, "Chaos-based image encryption using vertical-cavity surface-emitting lasers," *Optik*, vol. 176, pp. 119–131, 2019.
- [40] G. Alvarez and S. Li, "Some basic cryptographic requirements for chaos-based cryptosystems," *International Journal of Bifurcation and Chaos*, vol. 16, no. 08, pp. 2129–2151, 2006.
- [41] Y. Xu, H. Wang, Y. Li, and B. Pei, "Image encryption based on synchronization of fractional chaotic systems,"

- Communications in Nonlinear Science and Numerical Simulation*, vol. 19, no. 10, pp. 3735–3744, 2014.
- [42] F. Yang, J. Mou, C. Ma, and Y. Cao, “Dynamic analysis of an improper fractional-order laser chaotic system and its image encryption application,” *Optics and Lasers in Engineering*, vol. 129, Article ID 106031, 2020.
- [43] C. L. Li, Z. Y. Li, W. Feng, Y. N. Tong, J. R. Du, and D. Q. Wei, “Dynamical behavior and image encryption application of a memristor-based circuit system,” *AEU - International Journal of Electronics and Communications*, vol. 110, Article ID 152861, 2019.
- [44] B. Arpacı, E. Kurt, and K. Çelik, “A new algorithm for the colored image encryption via the modified Chua’s circuit,” *Engineering Science and Technology, an International Journal*, vol. 23, no. 3, pp. 595–604, 2020.
- [45] N. Tsafack, J. Kengne, B. Abd-El-Atty, A. M. Ilyasu, K. Hirota, and Abd El, “Design and implementation of a simple dynamical 4-D chaotic circuit with applications in image encryption,” *Information Sciences*, vol. 515, pp. 191–217, 2020.
- [46] F. Yu, H. Shen, Z. Zhang, Y. Huang, S. Cai, and S. Du, “A new multi-scroll Chua’s circuit with composite hyperbolic tangent-cubic nonlinearity: c,” *Integration*, vol. 81, pp. 71–83, 2021.
- [47] X. Li, J. Mou, S. Banerjee, Z. Wang, and Y. Cao, “Design and DSP implementation of a fractional-order detuned laser hyperchaotic circuit with applications in image encryption,” *Chaos, Solitons & Fractals*, vol. 159, Article ID 112133, 2022.
- [48] A. Sambas, S. Vaidyanathan, X. Zhang et al., “A novel 3D chaotic system with line equilibrium: multistability, integral sliding mode control, electronic circuit, FPGA implementation and its image encryption,” *IEEE Access*, vol. 10, pp. 68057–68074, 2022.
- [49] S. Vaidyanathan, A. Sambas, E. Tlelo-Cuautle et al., “A new 4-D multi-stable hyperchaotic system with No balance point: bifurcation analysis, circuit simulation, FPGA realization and image cryptosystem,” *IEEE Access*, vol. 9, pp. 144555–144573, 2021.
- [50] R. Gorenflo and F. Mainardi, “Fractional calculus: integral and differential equations of fractional order,” in *Fractals and Fractional Calculus in Continuum Mechanics*, A. Carpinteri and F. Mainardi, Eds., pp. 223–276, Springer, Berlin, Germany, 1997.
- [51] I. Podlubny and A. M. A. El-Sayed, “On two definitions of fractional calculus,” *Slovak Academy of science-institute of experimental physics*, vol. 3, 1996.
- [52] I. Podlubny, *Fractional Differential Equations*, Academic Press, Cambridge, CA, USA, 1999.
- [53] A. M. A. El-Sayed, “Fractional order diffusion-wave equation,” *International Journal of Theoretical Physics*, vol. 35, no. 2, pp. 311–322, 1996.
- [54] A. M. A. El-Sayed and F. M. Gaafar, “Fractional calculus and some intermediate physical processes,” *Applied Mathematics and Computation*, vol. 144, no. 1, pp. 117–126, 2003.
- [55] A. M. A. El-Sayed, “Fractional differential-difference equations,” *Journal of Fractional Calculus*, vol. 10, pp. 101–106, 1996.
- [56] A. M. A. El-Sayed, “Nonlinear functional differential equations of arbitrary orders,” *Nonlinear Analysis: Theory, Methods & Applications*, vol. 33, no. 2, pp. 181–186, 1998.
- [57] A. M. A. El-Sayed and F. M. Gaafar, “Fractional order differential equations with memory and fractional-order relaxation-oscillation model,” *Pure Mathematics and Applications*, vol. 12, pp. 296–310, 2001.
- [58] A. M. A. El-Sayed, A. E. M. El-Mesiry, and H. A. A. El-Saka, “Numerical solution for multi-term fractional (arbitrary) orders differential equations,” *Computational and Applied Mathematics*, vol. 23, no. 1, pp. 33–54, 2004.
- [59] A. M. A. El-Sayed, F. M. Gaafar, and H. H. Hashem, “On the maximal and minimal solutions of arbitrary orders nonlinear functional integral and differential equations,” *Mathematical Sciences Research Journal*, vol. 8, pp. 336–348, 2004.
- [60] A. M. A. El-Sayed, A. El-Mesiry, and H. A. A. El-Saka, “On the fractional-order logistic equation,” *Applied Mathematics Letters*, vol. 20, no. 7, pp. 817–823, 2007.
- [61] G. Hu, D. Xiao, Y. Wang, and T. Xiang, “An image coding scheme using parallel compressive sensing for simultaneous compression-encryption applications,” *Journal of Visual Communication and Image Representation*, vol. 44, pp. 116–127, 2017.
- [62] A. Sambas, S. Vaidyanathan, E. Tlelo-Cuautle et al., “A 3-D multi-stable system with a peanut-shaped equilibrium curve: circuit design, FPGA realization, and an application to image encryption,” *IEEE Access*, vol. 8, pp. 137116–137132, 2020.
- [63] A. A. Arab, M. J. B. Rostami, and B. Ghavami, “An image encryption algorithm using the combination of chaotic maps,” *Optik*, vol. 261, Article ID 169122, 2022.
- [64] Y. Sang, J. Sang, and M. S. Alam, “Image encryption based on logistic chaotic systems and deep autoencoder,” *Pattern Recognition Letters*, vol. 153, pp. 59–66, 2022.
- [65] Y. Wu, J. Noonan, and S. Aгаian, “NPCR and UACI randomness tests for image encryption,” *Cyber J: Multidiscip J Sci Technol J Sel Areas Telecommun (JSAT)*, vol. 1, pp. 31–38, 2011.